PLOS ONE

RESEARCH ARTICLE

Alkaloids of *Abuta panurensis* Eichler: *In silico* and *in vitro* study of acetylcholinesterase inhibition, cytotoxic and immunomodulatory activities

Rochelly da Silva Mesquita[1]*, Andrii Kyrylchuk[2], Regiane Costa de Oliveira[3], Ingrity Suelen Costa Sá[1], Gabriel Coutinho Borges Camargo[4], Gemilson Soares Pontes[3,4], Felipe Moura Araújo da Silva[5], Rita de Cássia Saraiva Nunomura[1], Andriy Grafov[6]*

1 Department of Chemistry, Federal University of Amazonas (UFAM), Manaus, Amazonas, Brazil, **2** Institute of Organic Chemistry, National Academy of Sciences (NAS), Kyiv, Ukraine, **3** Post-Graduate Program in Hematology, University of the State of Amazonas (UEA), Manaus, Amazonas, Brazil, **4** Laboratory of Virology, National Institute of Amazonian Research (INPA), Manaus, Amazonas, Brazil, **5** Analytical Center – Multidisciplinary Support Center (CAM), Federal University of Amazonas (UFAM), Manaus, Amazonas, Brazil, **6** Department of Chemistry, University of Helsinki, Helsinki, Finland

* rochellymesquita@gmail.com (RSM); andriy.grafov@helsinki.fi (AG)

Citation: da Silva Mesquita R, Kyrylchuk A, Costa de Oliveira R, Costa Sá IS, Coutinho Borges Camargo G, Soares Pontes G, et al. (2020) Alkaloids of *Abuta panurensis* Eichler: *In silico* and *in vitro* study of acetylcholinesterase inhibition, cytotoxic and immunomodulatory activities. PLoS ONE 15(9): e0239364. https://doi.org/10.1371/journal.pone.0239364

Editor: Alexandre G. de Brevern, UMR-S1134, INSERM, Université Paris Diderot, INTS, FRANCE

Received: March 10, 2020

Accepted: September 7, 2020

Published: September 29, 2020

Data Availability Statement: All relevant data are within the paper and its Supporting Information files.

Funding: European project Horizon 2020-MSCA-RISE-2016-734759, acronym VAHVISTUS; Finnish Center of Excellence in ALD; CAPES, PROCAD Amazônia, 88881.200581/201801; CNPq/MCT (CT-Amazônia Ed. No. 77/2013, proc. No. 408172/2013-4); FINEP; Foundation for Promotion of

Abstract

Natural products obtained from species of the genus *Abuta* (Menispermaceae) are known as ethnobotanicals that are attracting increasing attention due to a wide range of their pharmacological properties. In this study, the alkaloids stepharine and 5-*N*-methylmaytenine were first isolated from branches of *Abuta panurensis* Eichler, an endemic species from the Amazonian rainforest. Structure of the compounds was elucidated by a combination of 1D and 2D NMR spectroscopic and MS and HRMS spectrometric techniques. Interaction of the above-mentioned alkaloids with acetylcholinesterase enzyme and interleukins IL-6 and IL-8 was investigated *in silico* by molecular docking. The molecules under investigation were able to bind effectively with the active sites of the AChE enzyme, IL-6, and IL-8 showing affinity towards the proteins. Along with the theoretical study, acetylcholinesterase enzyme inhibition, cytotoxic, and immunomodulatory activity of the compounds were assessed by *in vitro* assays. The data obtained *in silico* corroborate the results of AChE enzyme inhibition, the IC_{50} values of 61.24μM for stepharine and 19.55μM for 5-*N*-methylmaytenine were found. The compounds showed cytotoxic activity against two tumor cell lines (K562 and U937) with IC_{50} values ranging from 11.77 μM to 28.48 μM. The *in vitro* assays revealed that both alkaloids were non-toxic to Vero and human PBMC cells. As for the immunomodulatory activity, both compounds inhibited the production of IL-6 at similar levels. Stepharine inhibited considerably the production of IL-8 in comparison to 5-*N*-methylmaytenine, which showed a dose dependent action (inhibitory at the IC_{50} dose, and stimulatory at the twofold IC_{50} one). Such a behavior may possibly be explained by different binding modes of the alkaloids to the interleukin structural fragments. Occurrence of the polyamine alkaloid

Research in the State of Amazonas - FAPEAM (Brazil). The funders had no role in study design, data collection and analysis, decision to publish, or preparation of the manuscript.

Competing interests: The authors have declared that no competing interests exist.

Abbreviations: 1D NMR, One-dimensional NMR; **2D NMR**, Two-dimensional NMR; **AChE**, acetylcholinesterase; **AChI**, acetylcholine iodide; **C18**, Octadecyl Carbon Chain; **COSY**, Correlated Spectroscopy; **DAD**, Diode Array Detection; **DEPT-135**, Distortionless Enhancement by Polarization Transfer; **DMSO**, dimethylsufoxide; **DTNB**, 5,5´-dithio-bis(2- nitrobenzoic)acid; **ELISA**, Enzyme-Linked Immunosorbent Assay; **FBS**, Fetal bovine serum; **HMBC**, Heteronuclear Multiple Bond Correlation; **HPLC**, High Performance Liquid Chromatography; **HRMS**, High Resolution Mass Spectrometry; **HSQC**, Heteronuclear Single Bond Correlation; **IC_{50}**, Half Minimal Inhibitory Concentration; **IL**, Interleukin; **LC-APCI-MS**, Liquid Chromatography—Atmospheric Pressure Chemical Ionization—Mass Spectrometry; ***m/z***, Mass-to-charge ratio; **MS/MS**, Tandem Mass Spectrometry; **MTT**, 3-(4,5-dimethylthiazol-2-yl)-2,5-diphenyltetrazolium bromide; **NMR**, Nuclear magnetic resonance; **PBMC**, peripheral blood mononuclear cells; **PBS**, Phosphate buffer saline; **PFP**, Pentafluorophenyl; **RMSD**, Root-mean-square deviation; **TMS**, Tetramethylsilane; **UCSF**, University of California, San Francisco; **UV**, Ultraviolet; **XRD**, X-ray diffraction; **μM**, micromolar.

5-*N*-methylmaytenine was reported for the first time for the Menispermaceae family, as well as the presence of stepharine in *A. panurensis*.

Introduction

Menispermaceae family has a wide geographic distribution, mainly in tropical and subtropical regions of the world; its name is related to a crescent moon shape of the seeds [1, 2]. The genus *Abuta* is native to tropical Central and South America, where it is represented by more than 30 species. Some of them have been used by indigenous people to prepare curare, alkaloid-containing arrow and dart head poisons that paralyze the prey [1, 3].

As a result, the Menispermaceae family have been in a focus of rising interest to study several classes of secondary plant metabolites, including alkaloids; which are rather abundant constituents [4–11]. Several classes of alkaloids were isolated from *Abuta*, those include: isoquinoline [12, 13], benzylisoquinoline [12, 14], benzyltetraisoquinoline [15], bisbenzyltetraisoquinoline [15–17], aporphine [18], and proaporphine [12, 15] derivatives; as well as other less frequent ones such as tropolone-isoquinoline, azafluoranthene, and benzazepine alkaloids [19, 20]. Those alkaloids reveal a wide range of pharmacological activities including muscle relaxant [1], antiplasmodial [14], inhibitory for acetylcholinesterase (AChE) and butyrylacetylcholinesterase enzymes [17, 21, 22], cytotoxic [19, 23, 24], and immunomodulatory [25].

A stepharine is one of the most representative proaporphine alkaloids in Menispermaceae family; it was first identified in the genus *Stephania* [26]. Proaporphine alkaloids are principally known for their potential to inhibit reversibly the acetylcholinesterase enzyme [27, 28]. Effectiveness and anti-AChE potential of the stepharine sulfate salt (stephaglabine) was reported for the treatment of traumatic and postoperative injuries of the peripheral nervous system and confirmed by a clinical study [29]. However, a pharmaceutical potential of stepharine is much wider according to the literature reports [30, 31]. It showed a cytotoxic activity against two human lung cancer cell lines [32], as well as a weak antifungal potential and DNA-damaging activity [30]. Therefore, both isolation of stepharine from plants cell cultures and several synthetic procedures were developed to satisfy a growing need for the medicinal use of the compound [31, 33].

Polyamine alkaloids (the derivatives of putrescine, spermidine, spermine, and cadaverine) are metabolites that occur widely in angiosperm plants [34–37], but are practically absent in sterile ones [35, 37–42]. Those compounds may also be isolated from other natural sources [43], particularly from fungi [44–48]. The polyamine alkaloids are not common for the Menispermaceae family, they were reported only for a *Cissampelos* genus [37, 49]. Cinnamoyl derivatives of polyamine alkaloids inhibit the AChE and α-glucosidase [38, 50, 51]. Alongside, they also inhibited cancer cell growth [46, 48, 52] and revealed an antiviral activity [53]. In the Amazon region, a polyamine alkaloid *N*,*N*'-di-*E*-cinnamoylspermidine or maytenine was isolated from *Maytenus krukovii (Maytenus chuchuhuasha)* trees (Celastraceae) [46, 54]. Several studies have stimulated the development of synthetic approach to that class of polyamides [46, 55–58] including the maytenine synthesis [59].

In the present study, 5-*N*-methylmaytenine (**1**) and the stepharine (**2**) were isolated for the first time from *A. panurensis*. This is also the first report on the occurrence of (**1**) in Menispermaceae family. Interactions of the alkaloids in question with acetylcholinesterase (AChE) enzyme and cytokines IL-6 and IL-8 were investigated *in silico* by molecular docking. The

potential of (**1**) and (**2**) as AChE inhibitors, antitumor and immunomodulatory agents was demonstrated by *in vitro* studies.

Materials and methods

Chemicals

Reagents and HPLC-grade solvents were purchased from Tedia Company (Fairfield, OH, USA) and Sigma-Aldrich and used as supplied. P.A. (Nuclear) grade solvents were purified by standard procedures used in natural products chemistry. An ultrahigh-purity water was obtained by Milli Q system (Millipore, Bedford, MA, USA).

Plant material

The authors declare that a specific permission from the National Institute of Amazonian Research (INPA) was required to collect plant material. The authors got the permission No. 35/12 of 02.12.2017 and confirm that the study did not involve endangered or protected species. *A*. *panurensis* plant material was collected at the Adolpho Ducke Forest Reserve, 26 km along the AM-010 highway from the city of Manaus, the State of Amazonas, Brazil. The species under investigation had been identified by the taxonomist L.S.Mergulhão. The voucher specimens were deposited in the Herbarium of the National Institute of Amazonian Research (INPA) under the voucher no 279373. The access to genetic heritage was registered at the National System of Genetic Heritage and Associated Traditional Knowledge Management (SisGen, Brazil) under the code number A9CC956.

The branches collected were dried at room temperature (ca. 20˚C) for 10 days. Subsequently, the vegetal material (1.4 kg of branches) was crushed in a knife mill and stored in a refrigerator until use.

Extraction

Dried and crushed plant material was subjected to an acid-base extraction [60]. The crushed branches (300g) were macerated with a 10% solution of NH_4OH (2L) and CH_2Cl_2 (2L) at room temperature (20˚C) for 72h, the material was stirred every 24 hours. The organic phase (1.5L) was transferred to a separatory funnel with a 10% solution of acetic acid (2L) and stirred manually. Then, the acidic aqueous phase was transferred to another vessel and the pH was adjusted to 10 using NH_4OH and extracted with CH_2Cl_2 (2 × 300mL). The CH_2Cl_2 phase was separated, concentrated on a rotary evaporator under reduced pressure, and dried with anhydrous sodium sulfate, resulting in the alkaloid fraction (280mg).

LC-APCI-MS analysis

LC-APCI-MS analyzes were performed on an Acella chromatograph (Thermo Scientific); coupled to a triple-quadrupole mass spectrometer model TSQ Quantum Acess® (Thermo Scientific), equipped with an Atmospheric Pressure Chemical Ionization (APCI) source, operated in positive mode with monitoring in the range of *m/z* 100–800. The mass spectrometer was equipped with Surveyor LC Pump Plus, Surveyor Autosampler Plus, Rheodyne injection valve (25μL), Luna C18 column (150 × 4.60mm, 5μm) (Phenomenex–Torrance, CA, USA), operating simultaneously with Surveyor PDA Plus diode array detector (DAD). The mobile phase was composed of B (methanol) and A (formic acid 1% v/v in H_2O) with a linear elution gradient: 0–20 min 20–80% B, 20–35 min 80% B, 35–45 min 20–80% B. The flow rate of the mobile phase was 1 mL/min and the injection volume was 10μL. The DAD detector was set up for

monitoring between 200-400nm. The spectra were processed using an Xcalibur software (version 2.2).

Semi-preparative HPLC analysis

Isolation of the alkaloids was performed on a semi-preparative scale on a Shimadzu chromatograph composed of a CBM-20A communication module, SPD-20AV UV detector, DGU-20A5 degasser, LC-6AD pump, 200 μL Rheodyne injection valve, and Luna C18 column (250 x 15.00mm, 5μm) (Phenomenex–Torrance, CA, USA) with a flow rate of 3 mL/min. The mobile phase was composed of B (methanol) and A (formic acid 1% v/v in H_2O), with a linear elution gradient: 0–20 min 20–80% B, 20–35 min 80% B, 35–45 min 20–80% B. The UV detector was set to monitoring at 260nm and 280nm. Fractions containing 5-*N*-methylmaytenine (11.2mg—**1**) and stepharine (22.1mg—**2**) were collected and analyzed by high-resolution mass spectrometry (HRMS) and NMR spectroscopy.

High resolution mass spectrometry

HRMS analyses were performed on a Shimadzu chromatograph composed of a CBM-20A communication module, a SPD-20AV UV detector, a LC-20AD pump, a SIL-20A HT autosampler (200μL), a CTO-20A oven, and a Luna PFP column (150 x 2mm, 100A); coupled to a Bruker microTOF-QII mass spectrometer, equipped with an Atmospheric Pressure Chemical Ionization (APCI) source, operated in a positive mode. The instrument parameters were as follows: capillary voltage, 4500V; nebulizer pressure (N_2), 4.0 bar; dry gas flow (N_2), 8L/min; dry heater temperature, 200˚C; with a monitoring in the range of *m/z* 100–800 Da. The mobile phase was composed of B (formic acid 0.1% v/v in methanol) and A (formic acid 0.1% v/v in H_2O) with a linear elution gradient as follows: 0–2 min 20–80% B; 2–42 min 100% B. The flow rate of the mobile phase was set to 0.2 mL/min and the injection volume was 10μL. The UV detector was set up for monitoring between 254nm and 330nm. The spectra were processed using a Bruker Compass Data Analysis software (version 4.2).

1D and 2D NMR spectroscopy

NMR spectra were recorded on a Bruker Avance IIIHD spectrometer, 500.13 MHz for ^{1}H and 125.0 MHz for ^{13}C operated at a magnetic field strength of 11.7 Tesla, equipped with a 5 mm direct detection PA BBO BBF HD-05-Z SP Intelligent probe incorporating Z-axis gradient coil, capable of providing gradient amplitudes up to 50 G/cm. Shigemi's 5.0 mm NMR tubes were used. For structural elucidation, the samples of 5-*N*-methylmaytenine and stepharine were solubilized in 600 μL of DMSO-d_6 (δ_H 2.50, δ_C 39.9) and CD_3OD (δ_H 3.34, δ_C 49.8), respectively. The acquisition of ^{1}H, ^{13}C, DEPT 135, COSY, HSQC, and HMBC spectra was performed using standard Bruker pulse sequences. The analysis based on ^{1}H NMR data was performed by solubilizing 10.0 mg of the 5-*N*-methylmaytenine in 550 μL of DMSO-d_6 with 50 μL of TMS (0.5 mM, 98%, Tokyo Chemical Industry) and 15.0 mg of the stepharine in 550 μL of CD_3OD with 50 μL of TMS (0.5 mM, 98%, Tokyo Chemical Industry) at 25 ˚C. Acquisition of 5-*N*-methylmaytenine and stepharine spectra was performed using the zg30 pulse sequence with water signal suppression, data points of the 64 kB time domain, 10 kHz spectral width, 1.00 second relaxation delay (D1), 3.27 second acquisition time (AQ), 32 scan numbers with DS of 2, decomposition resolution of 0.31 Hz, a constant receiver gain at 161 (5-*N*-methylmaytenine) and 181 (stepharine) with displacement frequency set at 2,425.23 Hz, PLW1 of 20.3 W. The calibration pulse (P1 9.400 μs to 5-*N*-methylmaytenine and P1 10.300 μs to stepharine) with PLW9 were of 7.183×10^{-5} W (5-*N*-methylmaytenine) and 8.6243×10^{-5} W (stepharine). Data were processed using Bruker® Topspin 4.0.6 software.

Molecular docking calculations

Ligand structures preparation. Ligand structures were built manually and preliminary optimized in a classic molecular mechanics software. In order to use equilibrium ligand structures, their geometry optimizations were conducted using a semi-empirical PM7 level [61] within the MOPAC program [62]. Ligand structure files for docking were prepared using AutoDock Tools [63, 64]. Default settings for the detection of rotatable bonds were used.

Protein files preparation. X-ray structures of the proteins under investigation (AChE, PDB ID: 6H12; IL-6, PDB ID: 4NI7 and IL-8, PDB ID: 3IL8) were obtained from the RCSB Protein Data Bank. *Missing residues*. Modeling of missing residues in the protein structures was performed using Modeller web-service [65]. Obtained structures that do not possess serious structural issues were selected for docking studies. Clashes or contacts between the side chains of the produced structures were resolved by minimization routine implemented in UCSF Chimera [66]. *Water molecules* are commonly found in the XRD structures of proteins and can have substantial impact on the docking affinities. Selection of water molecules that could be important in docking was performed according to the distance criterion. All water molecules farther than 3.3 Å from the H-bond donors and acceptors in the protein structures were removed. Protonation of the oxygen atoms in water molecules was made in UCSF Chimera followed by minimization of the hydrogen positions.

Binding sites of the proteins were identified using Discovery Studio Visualizer [67]. AutoDock Tools [63,64] were used for the preparation of Structure files for docking.

Docking runs. Docking studies were performed with AutoDock Vina program [68]. The protein structures stayed rigid during the docking in all cases. Each run generated nine binding poses. Exhaustiveness parameter of 50 was used for the medium search space sizes, e.g. for the binding pocket in AChE. In the case of larger search spaces (IL-6, IL-8) exhaustiveness of 500 was used. Since the success of a docking run depends on a random seed, which is defined at the beginning of the run and does not change during it; we have performed three docking runs for each protein-ligand pair and search space. The best docking poses found were similar between the runs in most cases, showing that the chosen parameters provided exhaustive search of the conformational space. *Missing residues*. Selected protein structures from Modeller service were used for the estimation of binding to the regions that were missing in the initial XRD structures. Search spaces that include the modeled parts of the protein were chosen. *Water molecules*. It is known that inclusion of all water molecules in the docking run can lead to erroneous results [69]. Therefore, trial docking runs were performed with an inclusion of one of the crystallization water molecules found in the XRD structures at a time. The water molecules were fixed during the docking run. The search space either covered the defined binding site of the protein or was centered on the water molecule and had a size of 20×20×20 Å.

Protein structure images were obtained using Discovery Studio Visualizer [67], PyMOL [70], and UCSF Chimera [66]. Detailed docking parameters are collected in the S1 File.

Acetylcholinesterase inhibition assay

Acetylcholinesterase enzyme from an electric ray *Tetronarce californica* (Sigma-Aldrich, USA) was used for the experiments. The *in vitro* AChE inhibition assay was performed in 96-well microplates according to the methodology proposed by Ellman *et al.* [71] (1961) and Senol *et al.* [72] (2015) with some modifications. The alkaloids were tested at concentrations of 2.8; 5.6; 11.2; 22.5; 45.0 and 90.0 μg/mL. Initially, 20 μL of each sample from the stock solution (1 mg/mL) were added and serial dilutions were performed. Then, 150 μL of a sodium phosphate buffer pH = 8 (0.1 mM), 20 μL of 5,5′-dithio-bis(2- nitrobenzoic)acid (DTNB, 0.0025 M), and

20 μL of the acetylcholinesterase enzyme (1 U/mL) were added subsequently to each well at 25 ˚C and left for 15 minutes. The reaction was initiated by addition of 10 μL of acetylcholine iodide (AChI) (0.1 M). Neostigmine (0.28–9.0 μg/mL) was used as a positive control.

A thiocholine formed by the enzymatic hydrolysis of the AChI, reacts with the DTNB giving rise to yellow 5-mercapto-2-nitrobenzoate anion. Concentration of the latter in each well was measured as absorbance at 405 nm using a 96-well microplate reader spectrophotometer (Biotek model ELX800). The transformation was monitored for 30 min at 5 min intervals. Inhibition curve was plotted as the inhibition percent *vs* concentration. All assays were performed in triplicate.

Cytotoxicity assay

The cytotoxicity of the alkaloids to different cell lines was evaluated by MTT (3-(4,5-dimethylthiazol-2-yl)-2,5-diphenyltetrazolium bromide) cell proliferation assay. The following cell lines were used for the evaluation: K562 (human chronic myelogenous leukemia, ATCC® CCL-243™), U937 (human histiocytic lymphoma, ATCC® CRL-1593.2™), HL60 (human acute promyelocytic leukemia, ATCC® CCL-240™), Vero (kidney epithelial cells extracted from an African green monkey *Chlorocebus* sp., ATCC® CCL-81™), and human peripheral blood mononuclear cells (PBMC) from healthy blood donors. The cell lines K562, HL60, and U937 were kindly donated by Prof. S.O. Saad (Hematology and Hemotherapy Center at the National Institute of Blood Science and Technology of the University of Campinas, Campinas, São Paulo, Brazil). The Vero cells were kindly donated by Prof. F.Naveca (Laboratory of Infectious Disease Ecology in the Amazon, L. and M.Deane Institute, FIOCRUZ, Manaus, Amazonas, Brazil). The cells were cultured in 96-well plates. An amount of 2×10^4 cells was seeded into each well containing 0.2 mL of a RPMI medium supplemented with 10% FBS, penicillin-streptomycin and fungizone, in an atmosphere of 5% CO_2 at 37˚ C for 24 hours. After a formation of sub-confluent monolayer, the cells were treated with different concentrations of the alkaloids (12 . . . 100 μg/mL) and incubated again at the same conditions for 24, 48, and 72 hours. Sterile PBS and DMSO 100% were used as negative and positive controls, respectively. Subsequently, the medium was removed from all wells and 10 μL of the MTT (5 mg/mL in sterile PBS) diluted in 100 μL of a DMEM medium (without phenol red to avoid misinterpretation) was added into the wells and incubated for 4 hours at the same conditions mentioned above. After that, the MTT was removed and 50 μL of the MTT lysis buffer were added to each well. The plate was homogenized gently to dissolve the formazan crystals and incubated for 10 minutes at 37 ˚C. Optical densities of the samples at wavelength of 570 nm were measured using a microplate reader. The relative viability of the cells was estimated using the following equation:

$$\frac{\text{A570 of treated sample}}{\text{A570 of untreated sample}} \times 100,$$

where A570 is the absorbance at 570nm. All assays were done in triplicate.

Immunological assay

To analyze the immunomodulatory potential, human peripheral blood mononuclear cells (PBMCs) obtained from healthy blood donor candidates were cultured in RPMI-1640 medium in a 96-well plate and incubated for 24h with 5-*N*-methylmaytenine (12.5 μM and 25 μM) or stepharine (28.48 μM and 57.0 μM). After the incubation, the supernatants were collected for cytokine assays. The supernatant of untreated PBMC cells was used as control. The concentrations of IL-6 and IL-8 cytokines were evaluated by commercially available enzyme-linked

immunosorbent assay (ELISA) kits (Boster, Pleasanton, CA, USA). The results were normalized for protein levels contained in each sample and were expressed in pg/mg of total protein. The assays were repeated in triplicate for each individual sample using untreated cells as negative control. This study was approved by the Committee for Ethics in Research on Human Beings of the HEMOAM (approval number: 3.138.343).

Statistical analysis

Statistical analysis was performed with GraphPad Prism 7.0® software using Student's *t*-test and ANOVA. A probability value of less than 0.05 was chosen as a statistical significance criterion. Throughout the text, the asterisks correspond to the following probability values: * means $p<0.01$; ** means $p< 0.001$; and *** means $p<0.0001$, when compared to the negative control (untreated cells). The half maximum inhibitory concentration IC_{50} values were calculated using nonlinear regression.

Results

Spectral data

5-*N*-methylmaytenine (**1**) was isolated as a light yellow amorphous solid (11.2 mg). ^{1}H NMR (500 MHz, DMSO d_6, TMS): δ 8.12 (t; 2H; *J* = 5.5 Hz, 1 and 10-NH), δ 7.56 (m, 2H, 5′-H and 5′′-H or 9′-H and 9′′-H), δ 7.54 (m, 2H, 9′-H and 9′′-H or 5′-H and 5′′-H), δ 7.55 (m, 2H, 6′-H, 6′′-H, 8′-H, 8′′-H), δ 7.40 (m, 2H, 7′-H and 7′′-H), δ 7.42 (m, 1H, 3′-H or 3′′-H), δ 7.38 (m, 1H, 3′′-H or 3′-H), δ 6.63 (d, 1H, 2.4 Hz, 2′-H or 2′′-H), δ 6.60 (d, 1H, 2.4 Hz, 2′′-H or 2′-H), δ 3.20 (m, 2H, 2-H), δ 3.18 (m, 2H, 9-H), δ 2.35 (m, 2H, 4-H), δ 2.32 (m, 2H, 6-H), δ 2.16 (s, 3H, 5-NCH_3), δ 1.61 (m, 2H, 3-H), δ 1.47 (m, 2H, 8-H), δ 1.45 (m, 2H, 7-H). ^{13}C NMR (125 MHz, DMSO d_6, TMS): δ 165.32; 165.27; 135.43; 127.98; 127.94, 129.39; 129.83; 138.85; 138.88; 122.79; 122.83; 55.26; 57.12; 42.09; 37.58; 39.07; 27.28; 24.53; 27.48 ppm. (S1 Table in S1 File). MS (APCI+) *m/z* 420 $[M+H]^+$: 202, 188, and 131. HRMS *m/z* 420.2669 (calc. for $C_{26}H_{34}N_3O_2$ *m/z* 420.2646, $\Delta_{m/z\ theor.}$ = -5.6 ppm).

Stepharine (**2**) was isolated as a light brownish amorphous solid (22.1mg). ^{1}H NMR (500 MHz, CD_3OD, TMS): δ 7.01 (dd, 1H, 3 and 10Hz, 12-H), δ 7.16 (dd, 1H, 3 and 10Hz, 8-H), δ 6.89 (s, 1H, 3-H), δ 6.41(dd, 1H, 1.8 and 10Hz, 11-H), δ 6.29 (dd, 1H, 1.8 and 10Hz, 9-H), δ 4.72 (m, 1H, 6a-H), δ 3.82 (s, 3H, 2-OCH_3), δ 3.70 (ddd, 1H, 1.5, 6.3 and 13Hz, 5-H), δ 3.61 (s, 3H, 1-OCH_3), δ 2.52 (dd, 1H, 6.6 and 12 Hz, 7-H), δ 2.42 (dd, 1H, 10.5 and 12Hz, 7ʻ-H), δ 3.44 (ddd, 1H, 6.3, 11 and 13Hz, 5-H), δ 3,02 and δ 3,00 (m, 2H, 4-H), δ 1.95 (s, 1H, NH) ppm. ^{13}C NMR by HSQC (125 MHz, CD_3OD, TMS): δ 153.63; 150.28; 112.15; 127.81; 126.74; 56.48; 55.37; 43.71; 59.95, 44.90; 43.71; 23.5 ppm. (S2 Table in S1 File). MS (APCI+) *m/z* 298 $[M+H]^+$: 281, 266, 250, 235, 161. HRMS *m/z* 298.1461 (calc. for $C_{18}H_{20}NO_3$ *m/z* 298.1438, $\Delta_{m/z\ theor.}$ = -7.9 ppm).

Binding with acetylcholinesterase of *Tetronarce californica* (TcAChE)

X-ray structure of the AChE from the electric ray *T. californica* was found in the RCSB Protein Data Bank under 6H12 code [73]. The crystal structure retrieved from the Data Bank represents the AChE adduct with a functionalized urea ligand. In order to verify robustness of the method, preliminary docking studies were conducted using the ligand structures obtained from the experimental XRD data. The best affinity of the ligand without the inclusion of water molecules reached -15.3 kcal/mol with a RMSD value of 4.03 Å compared to the ligand pose found in the crystal structure. Relatively high RMSD value can be explained by substantial internal mobility of the ligand molecule. Inclusion of 18 crystallization water molecules

increased the affinity value to -14.0 kcal/mol with comparable RMSD. In the case of fully hydrated pocket, many binding poses were found with similar affinity values, ranging from -13 to -14 kcal/mol. Some of those conformations showed better RMSD values reaching 2.2 Å. Screening of the water molecules failed to achieve interaction energies lower than those obtained for the empty binding pocket. Therefore, water molecules do not seem to play a substantial role in the binding of the urea ligand. Still, there was a possibility that hydration could be important for interactions with stepharine or 5-*N*-methylmaytenine. Therefore, it was considered for those ligands as well.

Two major binding sites were identified in the AChE structure–the main active site and the region near the modeled C-terminal loop (Fig 1). Consequently, we have conducted docking studies of these sites and a rear region that can possess smaller pockets (S32–S37 Figs in S1 File and the accompanying information).

Neostigmine is known as an efficient AChE inhibitor that was used as positive control in this study. According to the neostigmine docking results, the best affinity value was achieved for the main cavity of the enzyme and reaches -7.6 kcal/mol. The binding energies for the other sites were weaker by ca. 2 kcal/mol. Inclusion of water molecules did not produce any pronounced effect on the affinities and changed them by ca. 0.5 kcal/mol (S31 Fig in S1 File and the accompanying information).

5-*N*-methylmaytenine (**1**) preferably binds to the AChE active site with the affinity of -10.5 kcal/mol. Stepharine (**2**) fits well inside the AChE active site with the predicted binding affinity of -10.3 kcal/mol. Affinities of both ligands to the other sites were weaker by 2 . . .4 kcal/mol. Explicit inclusion of water molecules into the binding cavity had little effect on the binding strengths (S31 Fig in S1 File and the accompanying information).

Binding with interleukin-6

X-ray structure of human interleukin-6 (PDB ID: 4NI7) was used for the docking studies [74]. The structure contains a co-crystallized nucleic acid moiety that was removed prior to docking. During the signaling event, the IL-6 associates with the IL-6 receptor (IL-6r) and forms a complex. Then, the second receptor protein, *viz*. the gp130 glycoprotein, binds to the complex giving rise to a dimer; and the signaling is initiated [74–76]. X-ray structure of the interleukin-receptor complex (Fig 2B) was retrieved from the RCSB PDB (ID: 1P9M) [76].

According to the original paper [74], the IL-6 molecule possesses three binding sites, where the interactions with the receptor proteins and the second IL-6 molecule occur (Fig 2A). IL-6 –IL-6r interaction takes place at the Site 1, whereas the IL-6 interacts with the gp130 at the Sites 2 and 3. The IL-6 molecule does not have an apparent binding pocket. Four small binding pockets at the Sites 1 and 2 and several smaller pockets at the upper rim of the protein were identified. Since the pocket volume has never exceed 42 $Å^3$, the entire protein surface was considered for the docking calculations.

The strongest affinity of -7.9 kcal/mol was found for **1**, when the ligand interacted with two helices and a modeled loop at the IL-6 upper rim. Several other binding modes employed an interaction with a side surface of the two helices, including a π-stacking with both 5-*N*-methylmaytenine phenyl rings as well. Water molecules had also been screened for possible interactions with the docked ligand, but no significant effect was found (p 45 of the S1 File).

Stepharine (**2**) binds to the IL-6 with the affinity of -6.9 kcal/mol at the same site as 5-*N*-methylmaytenine. Again, water molecules did not provide any additional binding strength (p 45 of the S1 File).

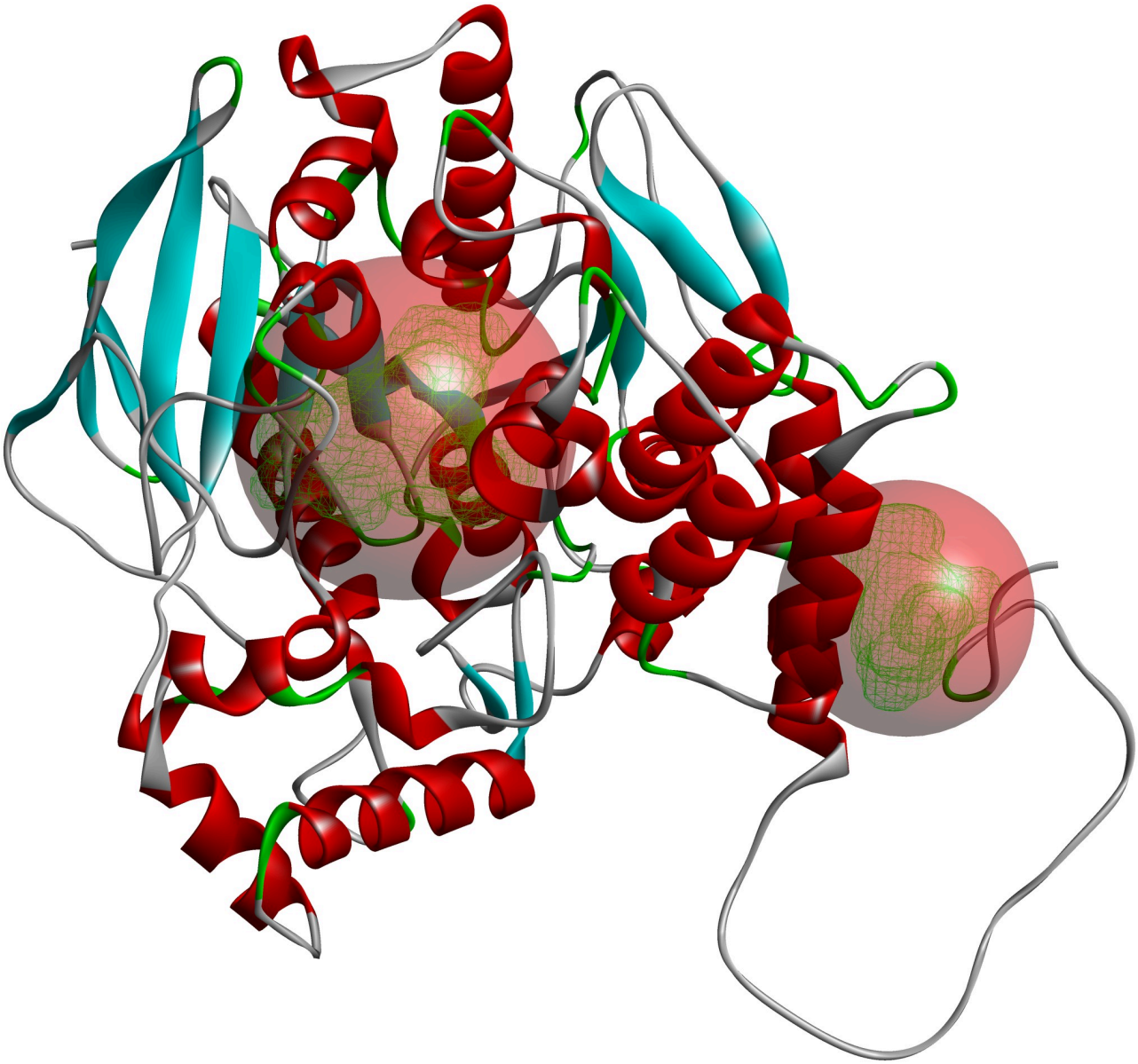

Fig 1. Two major binding sites found for AChE. Other, smaller sites are not shown.

https://doi.org/10.1371/journal.pone.0239364.g001

Interleukin-8

The crystal structure of the interleukin-8 was retrieved from the RCSB protein data bank (PDB ID: 3IL8) [77]. It is known that IL-8 interaction with the appropriate receptors (CXCR1 and CXCR2) involves two sites close to the N-terminus (Fig 3) [78–80]. The N-loop designated as Site I includes the residues from Ser14 to Lys20. The Site II is comprised of Glu4-Leu5-Arg6 ("ELR") residue sequence. During the signaling event, the Site I interacts with the receptor N-terminal residues while the Site II is involved in the interaction with the receptor extracellular residues [78]. Two other important regions of the protein structure comprise lateral sides of the α-helix and the β-strand involved in the IL-8 dimer formation.

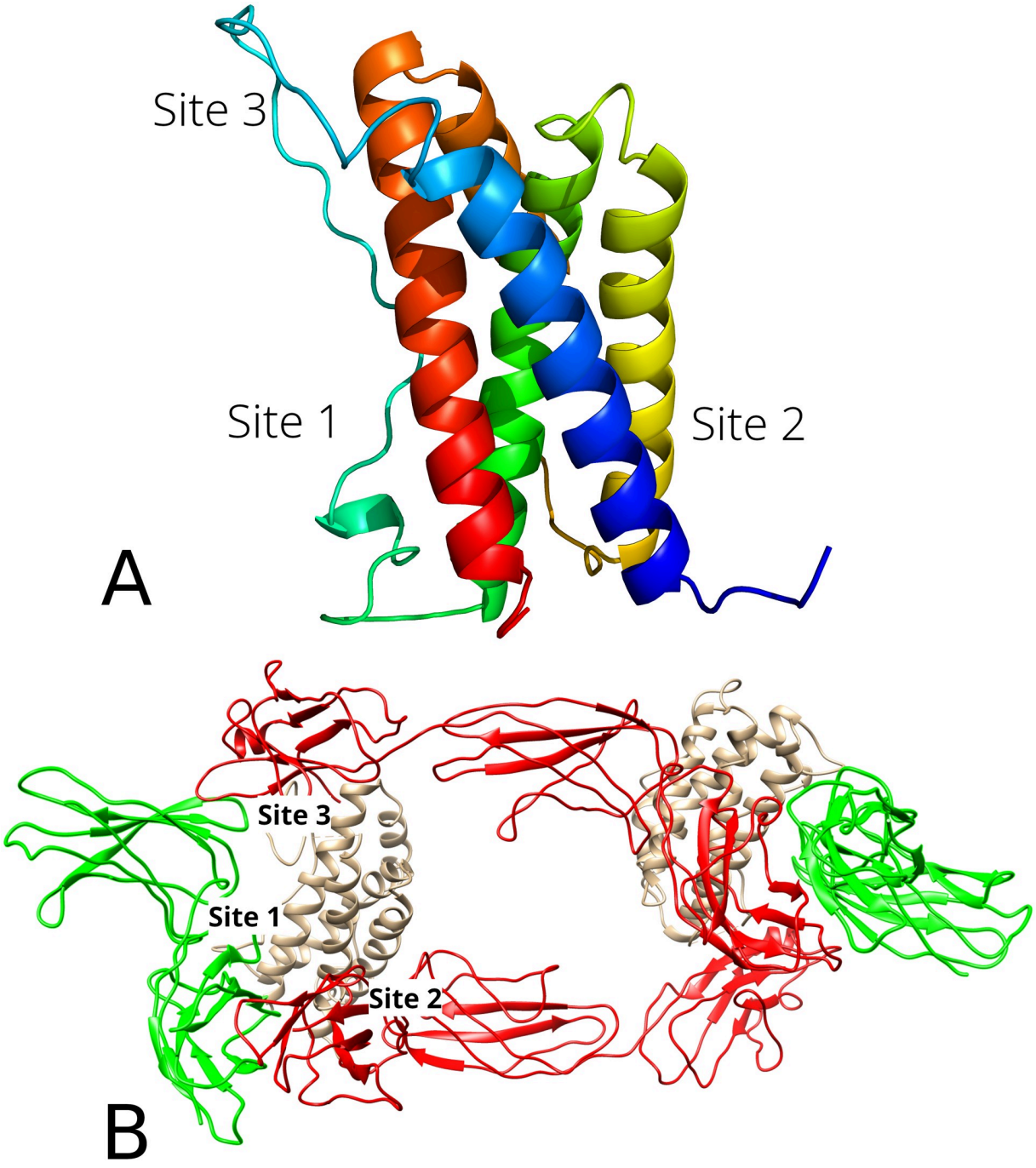

Fig 2. Binding sites of the IL-6 according to [74] (A) and IL-6 receptor complex 1P9M (B). In Fig 2B, the IL-6 structures are beige, the gp130 is marked red, and the IL-6r is green.

https://doi.org/10.1371/journal.pone.0239364.g002

No binding sites were identified by the Discovery Studio routines. Both the IL-8 monomer and dimer were employed in the docking studies. Due to a moderate size of the interleukin molecule, the entire surface of the protein was included into the search space. 5-*N*-methylmaytenine (**1**) interacts with the IL-8 monomer and dimer with the affinities of -6.9 and -7.0 kcal/mol, respectively. Stepharine (**2**) interacts with the monomeric and dimeric forms of the IL-8

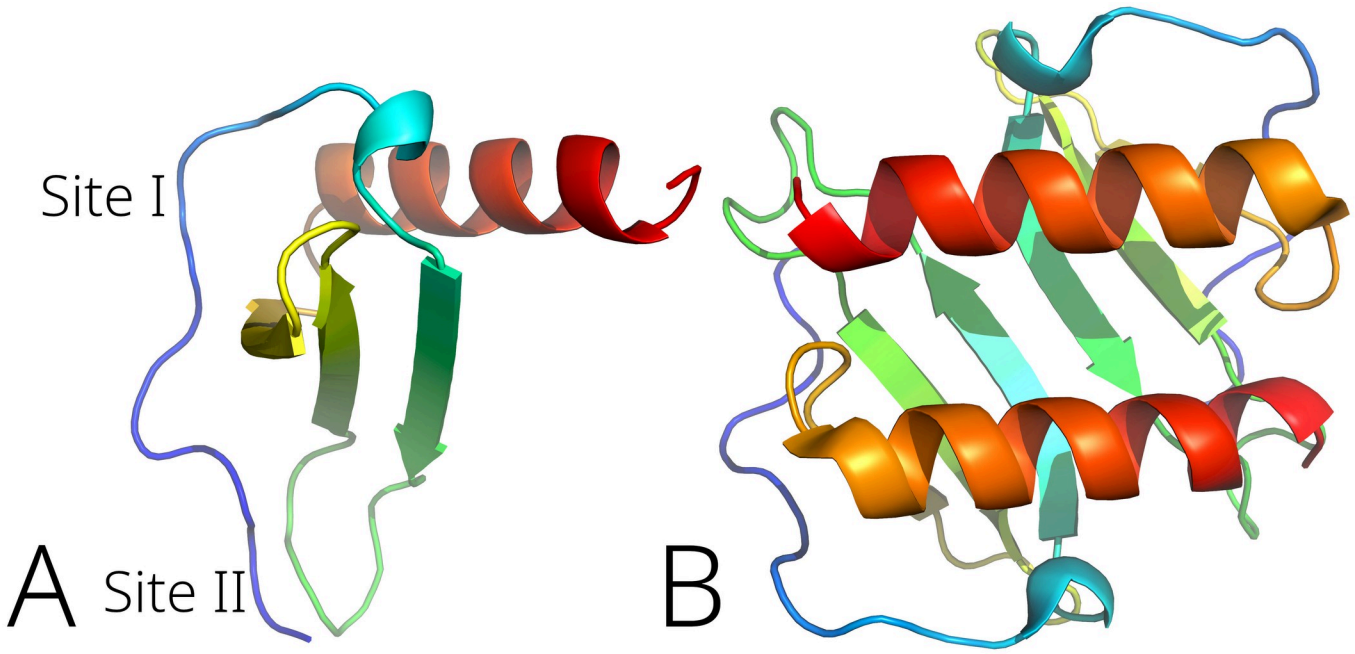

Fig 3. Binding sites of the IL-8 monomer according to [78–80] (A) and IL-8 dimer structure (B).

https://doi.org/10.1371/journal.pone.0239364.g003

with the similar affinity of -5.9 kcal/mol. Screening of the water molecules did not improve the binding strengths (S38 and S39 Figs in S1 File and accompanying information).

Acetylcholinesterase inhibition assay

The inhibitory activity of 5-*N*-methylmaytenine and stepharine towards the AChE enzyme showed the inhibition percentage of 78.01 ± 0.09% and, 74.58 ± 0.03% respectively. The inhibition percentage of 93.04 ± 0.03% was found for neostigmine, the efficient short-term reversible inhibitor of the AChE enzyme, used as a positive control. The compounds isolated from *A. panurensis* revealed promising IC_{50} values of 19.55μM for 5-*N*-methylmaytenine and 61.24μM for stepharine, the IC_{50} of 3.72μM was observed for neostigmine (Table 1).

Cytotoxicity assay

The compounds were screened for anticancer activity against three cancerous cell lines K562 (human chronic myelogenous leukemia), U937 (human histiocytic lymphoma), and HL60 (human acute promyelocytic leukemia). The compounds demonstrated a good

Table 1. Cytotoxic and AChE inhibitory activity of (1) and (2).

Compounds	IC_{50} (μM)			
	Cell lines			AChE
	K562	U937	HL60	
5-*N*-methylmaytenine	12.5	11.77	>100	19.55
Stepharine	28.48	19.97	>100	61.24
Neostigmine (positive control, AChE)	n/a	n/a	n/a	3.72

n/a–not applicable

https://doi.org/10.1371/journal.pone.0239364.t001

antiproliferative activity against the former two cell lines investigated. None of the compounds showed cytotoxicity against normal cells of the Vero line and human PBMC. The results for each compound are summarized in the Table 1.

Immunological assay

The levels of cytokines IL-6 and IL-8 were assessed by ELISA in the supernatant of human PBMC cells treated with 5-*N*-methylmaytenine and stepharine. Our results demonstrated that both 5-*N*-methylmaytenine and stepharine inhibited the IL-6 production in human PBMC after 24 hours treatment in levels statistically significant ($p = 0.0001$), when compared to the untreated PBMC. However, only stepharine induced significant ($p = 0.01$) decrease in the IL-8 levels, when compared to the control. It is interesting to note that the IL-8 levels became up-regulated in comparison to the control, when the concentration of 5-*N*-methylmaytenine was doubled to $2\times IC_{50}$ (Table 1). The results suggest that both **1** and **2** induce the anti-inflammatory modulation, but the effect on the IL-8 expression is dose-dependent in the former case.

Discussion

Spectral data interpretation

Structural formulas of the alkaloids with numbering of atoms are shown in the Fig 4. The MS and NMR spectra of both alkaloids are found in the S1 File.

Molecular formula of the compound (**1**) was determined by HRMS in the positive mode as $C_{26}H_{34}N_3O_2$. The ^{1}H NMR data revealed (Fig 4) the presence of two dehydroxylated cinnamic acid moieties characterized by signals of unsubstituted aromatic rings at δ_H 7.40 (m, H-7′and H-7′′) and δ_H 7.54–7.56 (m, H-5′; H-5′′; H-6′; H-6′′; H-8′; H-8′′; H-9′; H-9′′), as well as the signals of methylene protons at δ_H 7.38 (m, H-3′′ or H-3′), δ_H 7.42 (m, H-3′or H-3′′), δ_H 6.60 (d, H-2′or H-2′′), and δ_H 6.63 (d, H-2′′ or H-2′). The presence of an amide group in the structure was confirmed by the signal at δ_H 8.12 (-NH). Signals of proton resonances in the aliphatic region (δ_H 1.45–3.20) were also elucidated (S3 and S4 Figs in S1 File).

The presence of two cinnamamide moieties in the structure was confirmed by the HMBC experiment (Fig 4). The signals at δ_H 7.38 (m, H-3′′ or H-3′) and δ_H 7.42 (m, H-3′or H-3′′) show J^3 couplings to the quaternary carbon signals at δ_C 165.27 (C-1′or C-1′′) and δ_C 165.32 (C-1′′ or C-1′) indicate a presence of two carbonyls in the structure (S9 and S10 Figs in S1 File). Additionally, the HMBC spectra also showed correlations of the -NH group (δ_H 8.12) with the above mentioned carbonyl signals (δ_C 165.27 and δ_C 165.32) that confirm the presence of two cinnamamide moieties.

In the aliphatic region of the ^{13}C NMR spectra (S5 and S8 Figs in S1 File), the presence of a methyl (δ_C 42.09) and seven methylene carbons (δ_C 24–55) was confirmed by DEPT-135 (S13 and S14 Figs in S1 File). The methyl group (δ_C 42.09) directly linked to the nitrogen in the aliphatic chain can be confirmed in the HMBC with the long-distance proton couplings between the δ_H 2.16 (s, NCH_3) and the methylene carbons at δ_C 55.26 (C-4) and δ_C 57.12 (C-6).

Seven well-defined signals of methylene carbons were found in the aliphatic region of the ^{13}C NMR spectrum. The corresponding ^{1}H-^{13}C correlations were confirmed in the HSQC spectrum (S11 and S12 Figs in S1 File), where isochrony of two hydrogen atoms was demonstrated by the correlation of the proton resonance at δ_H 1.47 with two different carbon signals at δ_C 24.53 and δ_C 27.48. Furthermore, the proposed structure was confirmed by the following ^{1}H-^{1}H correlations in the COSY spectrum (Fig 4): δ_H 2.32 with δ_H 1.45; δ_H 2.35 with δ_H 1.61; δ_H 3.18 with δ_H 1.47, and δ_H 3.20 with δ_H 1.61 (S15 and S16 Figs in S1 File).

The MS/MS spectrum of the compound (**1**) is in agreement with the above NMR data. The ion *m/z* 420 showed sequential losses of 218 Da (*m/z* 202), 14 Da (*m/z* 188), and 57 Da (*m/z*

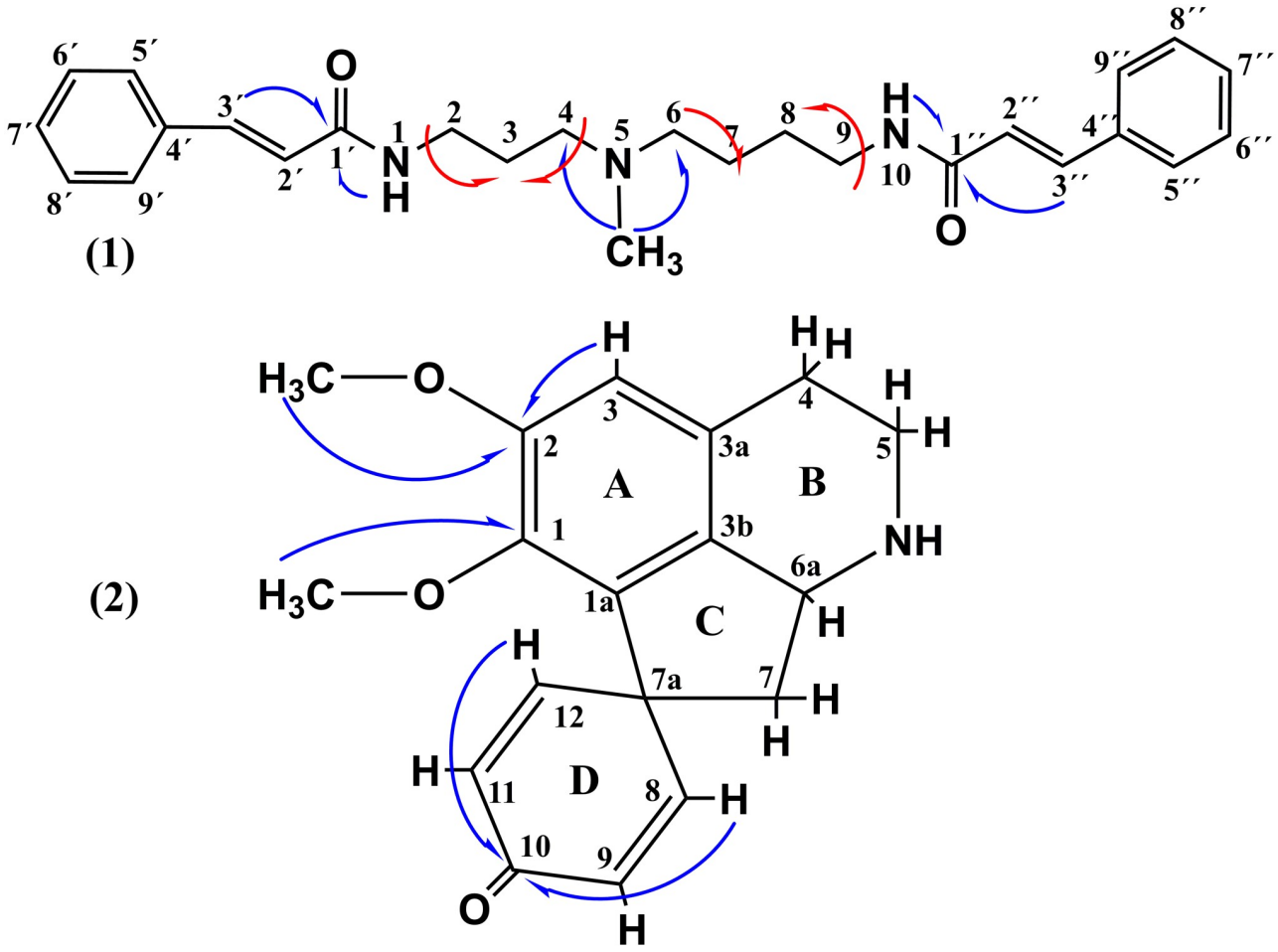

Fig 4. 5-*N*-methylmaytenine (1) and stepharine (2). Principal couplings are shown with arrows: HMBC–blue, COSY–red.

https://doi.org/10.1371/journal.pone.0239364.g004

131) (S1 Fig in S1 File), typical for the fragmentation pattern of cinnamic acid amides [46, 59]. Therefore, the compound (**1**) was identified as 5-*N*-methylmaytenine, i.e. 1,10-di-*E*-cinnamamide of 5-*N*-methylspermidine.

The compound (**2**) appeared as a light brownish amorphous solid. The molecular formula was determined by HRMS in positive mode as $C_{18}H_{20}NO_3$. The MS/MS spectrum of the *m/z* 298 ion showed sequential losses of 17 Da (*m/z* 281) and 15 Da (*m/z* 266), and a loss of 31 Da (*m/z* 281 → 250) (S17 Fig in S1 File); which are consistent with aporphine alkaloids containing adjacent methoxyls in the ring A and the non-substituted ring D [60, 81] (Fig 4).

The ^{1}H NMR spectrum is in agreement with the MS data. It exhibited signals typical for proaporphine alkaloids at δ_H 2.52 (dd; 6.6 and 12 Hz; H-7 or H-7′), δ_H 2.42 (dd; 10.5 and 12 Hz; H-7′or H-7), δ_H 3.02 (m; H-4), δ_H 3.44 (ddd; 6.3, 11, and 13 Hz; H-5 or H-5′) e δ_H 3.70 (ddd; 1.5, 6.3, and 13 Hz; H-5′or H-5). The following signals were observed in the range of aromatic proton resonances: δ_H 6.89 (s, H-3) corresponding to an *orto*-substituted ring A; δ_H 7.16 (dd; 3 and 10 Hz; H-8), δ_H 6.29 (d; 1.8 and 10 Hz; H-9), δ_H 6.41 (dd; 1.8 and 10 Hz; H-11), and δ_H 7.01 (dd; 3 and 10 Hz; H-12) characteristic of the unsubstituted ring D; and two signals δ_H 3.61 (s, 3H) and δ_H 3.82 (s, 3H) of the methoxy-substituents in the ring A (Fig 4 and S19-S21 Figs in S1 File).

The proaporphine alkaloid structure was proposed based on the HMBC experiments (Fig 4). The signals at δ_H 7.16 (dd; 3 and 10 Hz; H-8) and δ_H 7.01 (dd; 3 and 10 Hz; H-12) showed a J^3-coupling to the carbon at δ_C 186.6 (C-10). The proaporphine skeleton was also established following long-distance ^1H-^{13}C couplings of the signals at δ_H 6.89 (s, H-3) and those of the methoxyls at δ_H 3.61 (s, 3H) and δ_H 3.82 (s, 3H) with the carbons at δ_C 144.6 (C-1) and δ_C 154.7 (C-2), thus confirming the existence of two substitutions in the A ring (S24 and S25 Figs in S1 File). Therefore, the compound (**2**) was elucidated as being the proaporphine alkaloid stepharine.

The compounds were identified by a comparison of the obtained spectral results with data reported in the literature [46, 59, 82]. The alkaloid (**1**) was identified as 5-*N*-methylmaytenine, this is the first report on isolation of this compound from a natural product, as well as the first occurrence of the alkaloid in the Menispermaceae family [59].

The proaporphine alkaloid stepharine (**2**) was also described by us for the first time in *A. panurensis*. Previously, its presence was reported in *Stephania* genus [83–89], as well as in some *Abuta* species [4, 15].

Acetylcholinesterase inhibition

The docking study provided a very useful tool in the interpretation of the AChE inhibitory activity results, indicating that molecules under investigation were able to bind effectively to the TcAChE enzyme active site.

The neostigmine (used as a positive control in the assay) forms π-stacking interactions with the aromatic rings of amino acids from the so-called anionic subsite of the enzyme corresponding to the choline-binding pocket (Trp84 and Phe330). The stronger one is formed with the phenyl ring of Trp84 (3.66 Å). The stacking distance to Phe330 is 4.31 Å implying a weaker interaction. There exist two attractive Coulomb interactions as well. The first one is between the positively charged quaternary ammonium nitrogen and a carboxylic group of the Glu199. The second interaction is formed between the same charged nitrogen atom and a phenyl ring of the Trp84, at a distance of approximately 4.4 Å, typical for tetraalkylammonia–π interactions [90] (Fig 5).

Because the active site pocket of the acetylcholinesterase forms a deep and narrow gorge, formed of aromatic residues by 40% [91], the hydrophobic interactions play a major role in binding of the compounds under investigation to the AChE (Figs 5 and 6). Docking data indicate that (**1**) is a plausible ligand for the AChE, which can adopt a variety of binding poses due to its conformational flexibility. One of the cinnamic acid phenyls is sandwiched between two aromatic residues of the enzyme Trp84 and Phe330 at the distance of 3.6Å. . .3.9Å that is slightly above a typical value for a parallel displaced π-stacking. Interactions with peripheral subsites Tyr121 and Gly117 were also observed. Stepharine (**2**) fits well inside the AChE pocket with the predicted binding affinity of -10.3 kcal/mol. This energy corresponds to substantial interaction between the ligand and the enzyme. (Fig 6). π-Stacking is again the major protein-ligand interaction for this compound (3.66 Å with Trp84 pyrrole and 4.09 Å with Phe330 phenyl rings). Both alkaloids have their binding poses at the lipophilic anionic subsite (Trp84 and Phe330) of the TcAChE (Fig 6), where they are able to interact with the enzyme pocket [91, 92].

Overall, all three compounds studied (**1**, **2**, and neostigmine) have phenyl rings as the most important structural features that lead to similar interactions guiding their affinity towards the AChE. The preferential interaction of the neostigmine quaternary nitrogen with the π electrons of the aromatic rings at the binding site of the enzyme indicates greater affinity of that subsite towards easily polarizable ammonium ligands. [93]. The alkaloids in question have no

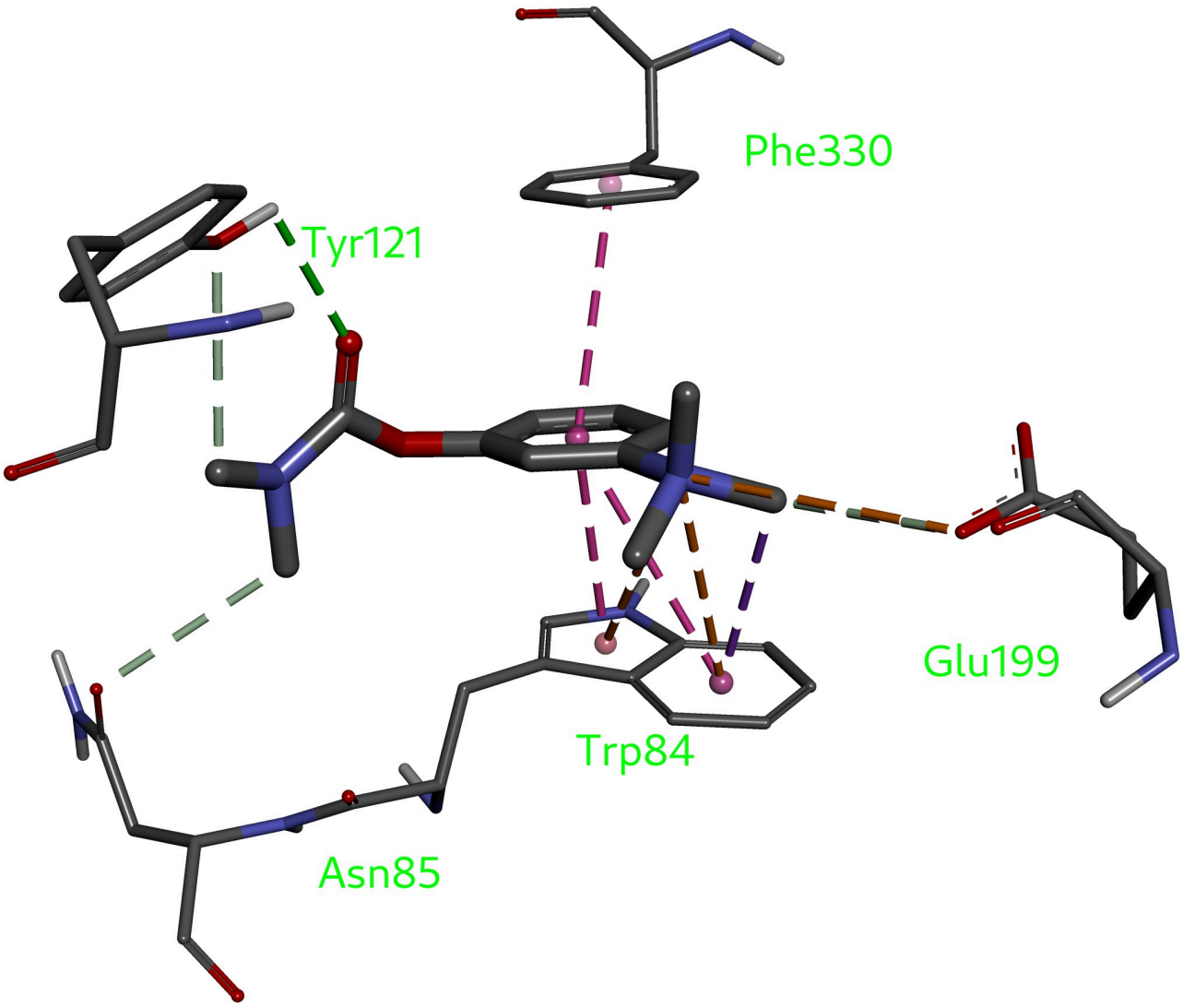

Fig 5. Neostigmine interactions with the AChE binding pocket.

https://doi.org/10.1371/journal.pone.0239364.g005

such moieties, which can be a reason for higher IC_{50} values of the **1** and **2**, than that of neostigmine.

Peripheral anionic binding site of the enzyme is also associated with the AChE-mediated abnormal β-amyloid protein aggregation in Alzheimer's disease patients [94, 95]. It is interesting to note that owing to a conformational flexibility of the molecule, 5-*N*-methylmaytenine interacts simultaneously with both the anionic and the peripheral subsites of the enzyme. Therefore, **(1)** may well be capable to have greater pharmacological potential [94], when compared to stepharine that interacts with the anionic active subsite only.

Currently, natural products constitute one of the main sources of the AChE inhibitors, used as active compounds to treat damages to central and peripheral nervous system, as well as to alleviate symptoms of neurodegenerative diseases [28, 96, 97]. Bisbenzylisoquinoline and protoberberine alkaloids exhibit a moderate AChE enzyme inhibition potential with IC_{50} values in the range of 34.66μM to 78.22μM [17] and 36.6μM to 141.8μM [98], respectively. Whereas aporphine and proaporphine alkaloids demonstrate better AChE inhibitory activity with the

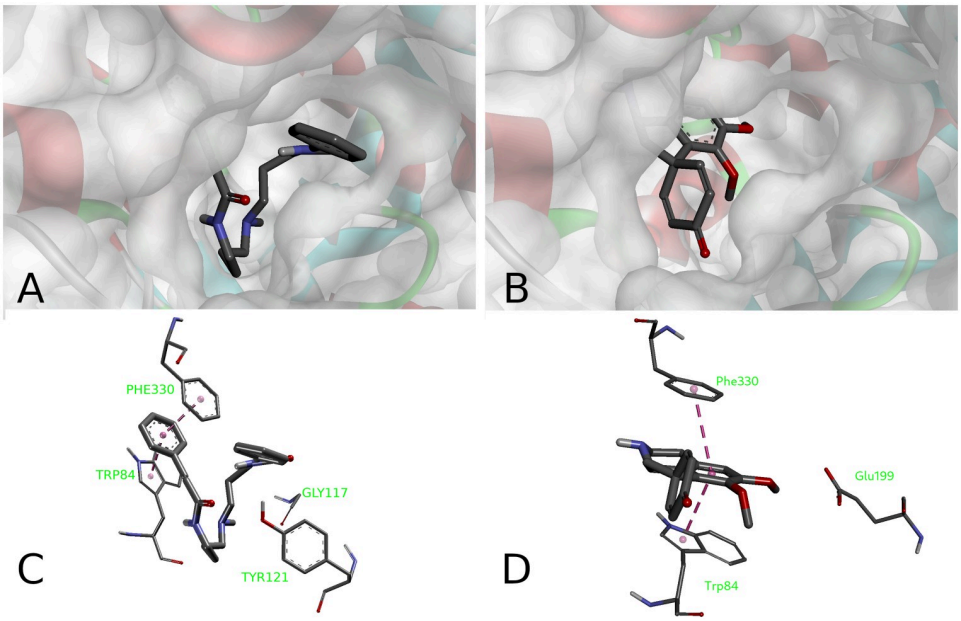

Fig 6. Binding poses (A, B) of the alkaloids inside the AChE pocket and their binding modes (C, D). 5-*N*-methylmaytenine (A, C) and stepharine (B, D).

https://doi.org/10.1371/journal.pone.0239364.g006

IC_{50} values ranging from 2.98μM to 20.4μM and this effect is often related to different substituents in their structure [27]. Polyamine alkaloids such as putrescine, spermidine, spermine, cadaverine, and their derivatives are present ubiquitously in all living cells; they have a variety of functions inside the cell, including the cell growth and regeneration [99]. For the central nervous system in particular, studies show that polyamines act on receptors related to neurodegenerative processes [100, 101]. For example, the spermidine decreases significantly the AChE activity, oxidative stress and neuroinflammation in a cerebral hippocampus [102].

Our study of two alkaloids first obtained from *A*. *panurensis* revealed that both compounds are promising AChE enzyme inhibitors. The capability of 5-*N*-methylmaytenine to interact simultaneously with several subsites in the enzyme structure may provide an important guideline in the search for new active compounds for treatment of neurological disorders [103].

Cytotoxicity assay

Effectiveness of 5-*N*-methylmaytenine (Fig 7) and stepharine (Fig 8) in different concentrations were evaluated against U937 and K562 tumor cell lines. The U937 cells were more susceptible to the stepharine anticancer action. Interestingly, the stepharine demonstrated higher cytotoxic activity against the K562 strain only in the first 24 hours of treatment. This result suggest that K562 cell line is more resistant to the stepharine treatment than U937. Both compounds showed practically no toxicity to non-cancerous cells (Vero and human PBMC, Fig 9).

Although stepharine showed greater stability of action in the course of the assay, the 5-*N*-methylmaytenine demonstrated higher efficiency, according to the IC_{50} values.

The results obtained corroborate well with the literature reports that isoquinoline alkaloids of different backbones, such as berberine and aporphine ones containing an oxo-substituent in their structure, particularly oxoisoaporphines, demonstrate moderate to strong potential for cytotoxic activity against several tumor cell lines, including those used in the present work [96, 104–107].

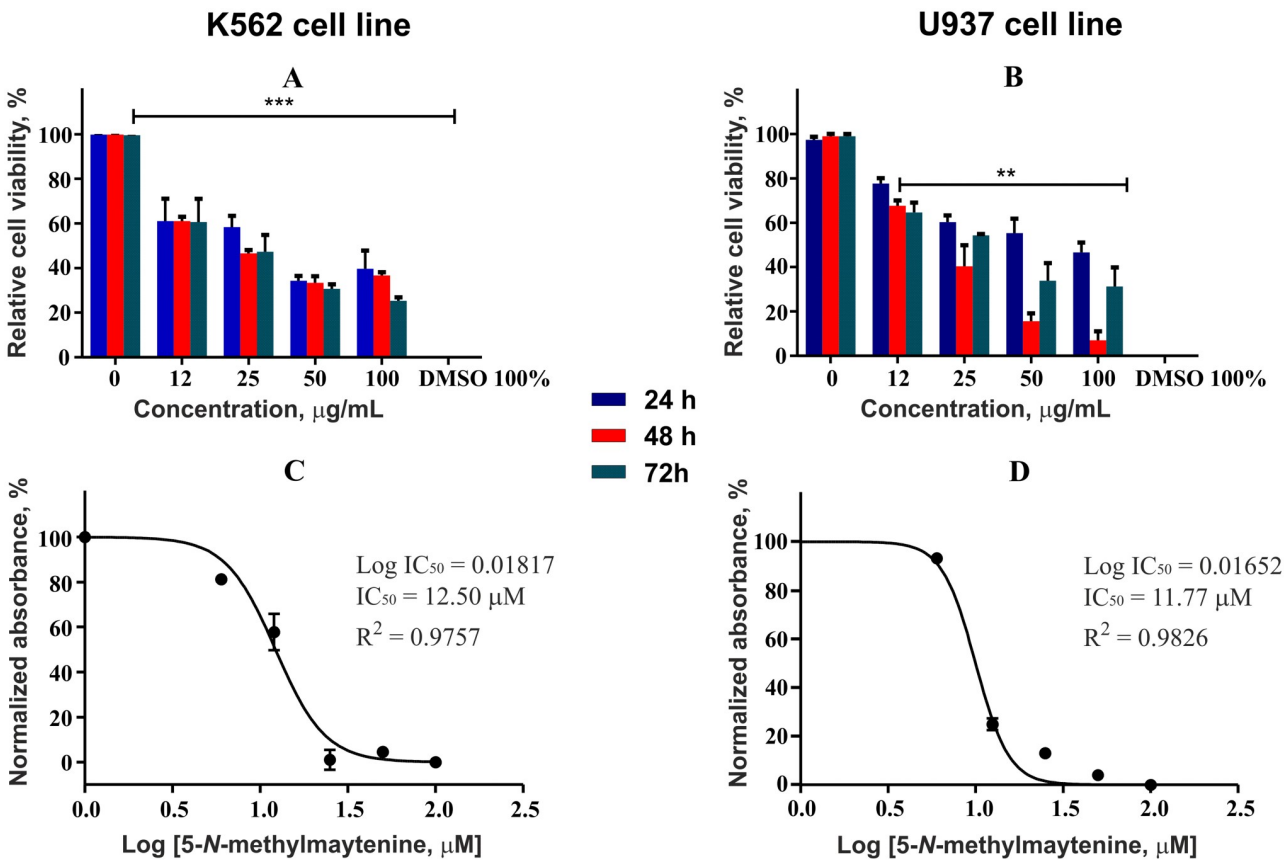

Fig 7. Cytotoxic activity of 5-*N*-methylmaytenine respective IC_{50} values.

https://doi.org/10.1371/journal.pone.0239364.g007

Immunomodulatory assay

The anti-inflammatory properties of acetylcholinesterase inhibitors are mediated by a cholinergic system present in the immune cells [108, 109]. For instance, macrophages and T cells express α7 homopentameric nAChR receptor that can down-regulate the production of inflammatory cytokines (TNF-α and IL-1β) and NF-κB-dependent transcription, when stimulated [110]. The latter pathway regulation may be involved in the pathogenesis of many chronic diseases such as asthma, rheumatoid arthritis, atherosclerosis, and even though the Alzheimer's disease [111–113]. In this study, we did not assess the potential of stepharine and 5-*N*-methylmaytenine in regulating the NF-κB immune pathway. However, our findings demonstrate that the cholinergic anti-inflammatory pathway could reduce the production of IL-6 and IL-8 owing to the AChE inhibitor treatment, which can protect against the damage provoked by inflammation in different types of inflammatory diseases.

According to the molecular docking studies, both alkaloids bind to the interleukins with quite similar affinity in the range of -8 . . .-6 kcal/mol.

Binding to the IL-6. In the case of IL-6, 5-*N*-methylmaytenine binds to the upper rim of the protein (Fig 10), giving rise to hydrogen bonds with carboxylic groups of Glu36 (modeled loop, 2.20 Å) and Asp145 (1.94 Å). A weak cation-π interaction with Arg89 guanidine moiety and favorable hydrophobic interactions between the phenyl ring of **1** and carbon chains of Leu42 and Lys39 were also formed.

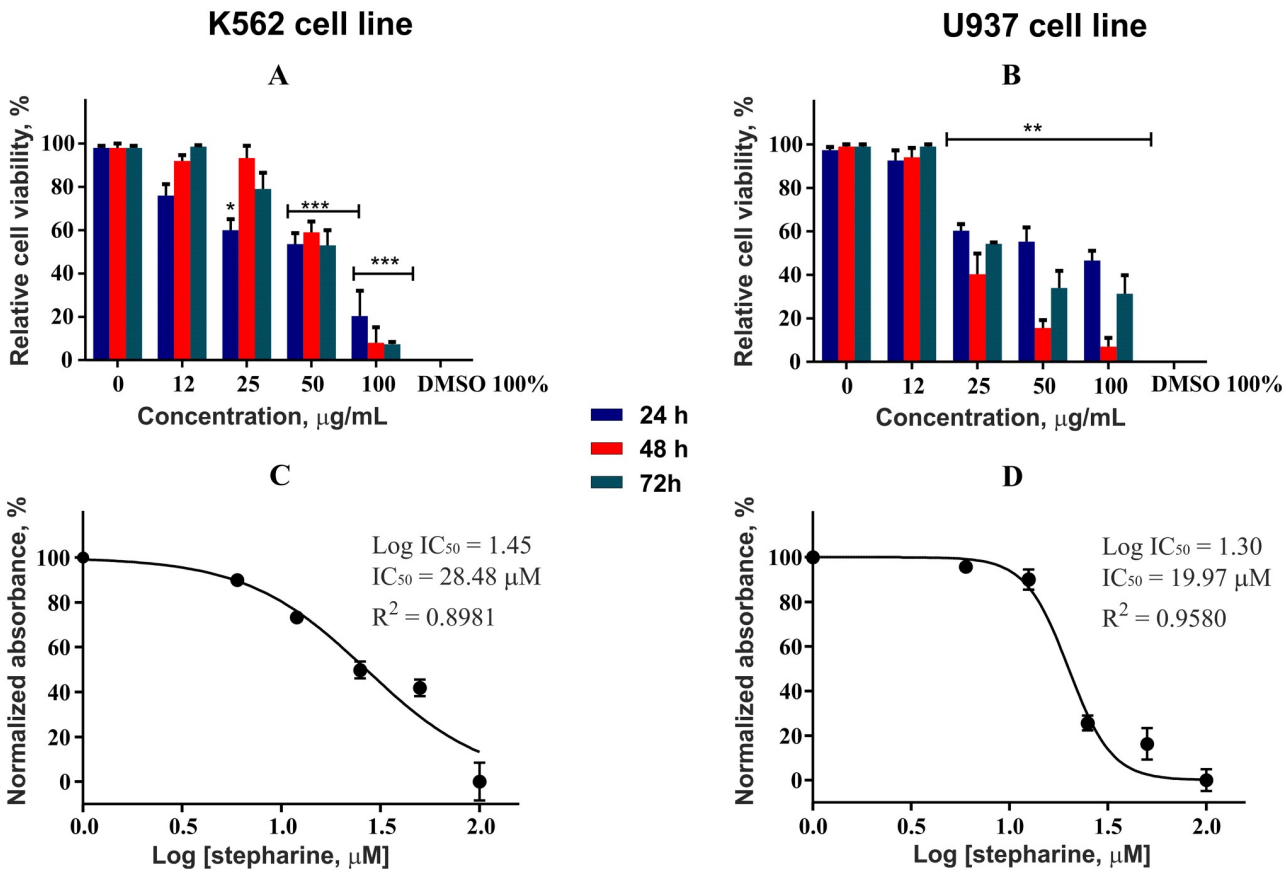

Fig 8. Cytotoxic activity of stepharine and respective IC_{50} values.

https://doi.org/10.1371/journal.pone.0239364.g008

Similarly, stepharine (**2**) binds to the top region of the IL-6 interacting with Met146 of the α-helix (π-sulfur interaction at 3.65 Å) and with Glu36 of the modeled loop (weak anion-π interaction with the carboxyl group).

Both alkaloids interact with the Site 3 of the IL-6 (Fig 2) indicating that they are able to disrupt IL-6 –gp130 complex formation and thus hinder the signaling. Results of the immunological assay are in agreement with the above statement (Fig 11).

Binding to IL-8. According to the docking results, both alkaloids bind into a shallow pocket between a Thr12 –Pro19 loop and a β-sheet region Ile40 –Cys50 (Fig 12), which are close to the receptor-binding Site I (Fig 3); implying inhibitory action of both **1** and **2**. 5-*N*-methylmaytenine forms an aromatic interaction with the Phe21 phenyl ring and two π-charge interactions with the Arg47 guanidine moiety of and the Asp45 carboxyl group. Stepharine binds to the protein pocket in a similar way by π-π stacking interaction with Phe21, but acts as a hydrogen-bond acceptor for the -NH proton of Arg47 (Fig 12). This fact may suggest a slightly stronger inhibition of IL-8 production by stepharine. In the case of 5-*N*-methylmaytenine, the induction of the IL-8 level downregulation seems to happen in a dose-dependent manner (Fig 11).

It was shown that some interleukins, including the IL-8, can exist both as dimers and monomers in solution [78]. The dimerization occurs at higher IL-8 concentrations and is highly sensitive to solution conditions such as pH and ionic strength [114, 115]. In general, affinity to the receptors and activity of the dimers are much lower than those of the monomers

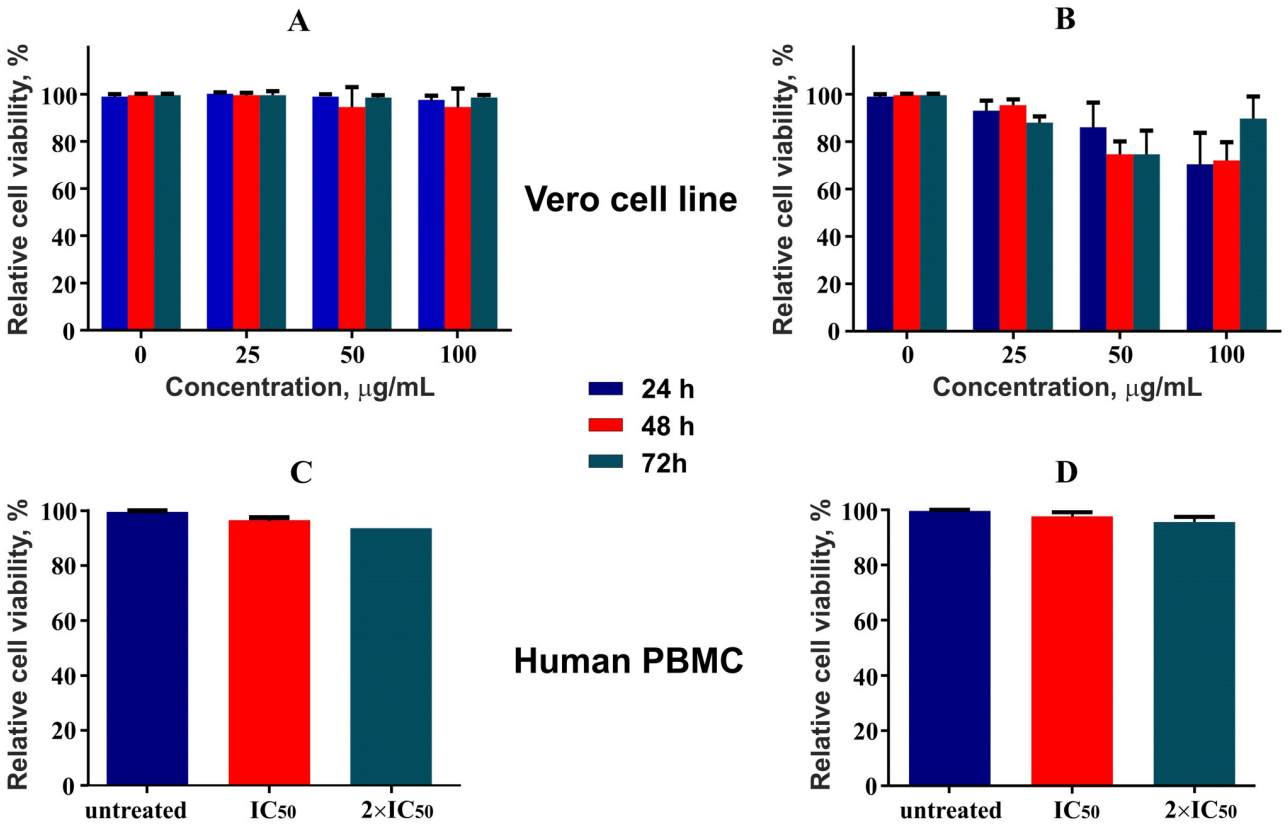

Fig 9. Cytotoxicity assessment of the alkaloids to Vero and human PBMC cells. Stepharine (A, C) and 5-*N*-methylmaytenine (B, D).

https://doi.org/10.1371/journal.pone.0239364.g009

[114, 116]. We conducted docking studies of 5-*N*-methylmaytenine and stepharine to the IL-8 dimer (Fig 13).

Affinities of the **1** and **2** to the dimer are similar to those of the monomeric protein: -7.0 kcal/mol for **1** and -5.9 kcal/mol for **2**. Inclusion of water molecules into the dimer structure did not lead to improvement of binding affinities. It is interesting to note that binding positions of the two ligands became different. While stepharine binds to the dimer the same way as it interacts with the monomer (Fig 12), the 5-*N*-methylmaytenine molecule is stretched between α-helices and interacts with both monomer moieties. Most of the direct interactions were found with one of the IL-8 units, *viz*., two hydrogen bonds with oxygen atoms of Asn71 and Glu70 (2.71 Å and 2.38 Å, respectively) and a weak anion-π interaction between the phenyl ring of **1** and a carboxylic group of Glu63 (3.85 Å). Carbon chains of Lys54 and Leu66 of another IL-8 molecule form hydrophobic interactions with the phenyl rings of 5-*N*-methylmaytenine. At lower concentrations, **1** is able to interact with the IL-8 dimers and possibly to prevent their dissociation into more active monomer form. At higher concentrations, the binding of 5-N-methylmaytenine to the IL-8 monomers and their activation may take place.

Mostly, IL-6 and IL-8 play a crucial role in the selective chemotaxis, degranulation, and activation of neutrophils. High levels of those interleukins are associated with an immunopathogenesis of many chronic inflammation diseases, such as cell injury in kidney inflammation, poor outcome of different neurological manifestations, and excessive infiltration of neutrophils in airways of cystic fibrosis patients [117–119]. Thus, therapies targeting pro-inflammatory cytokines, such as IL-6 and IL-8, have important clinical implications.

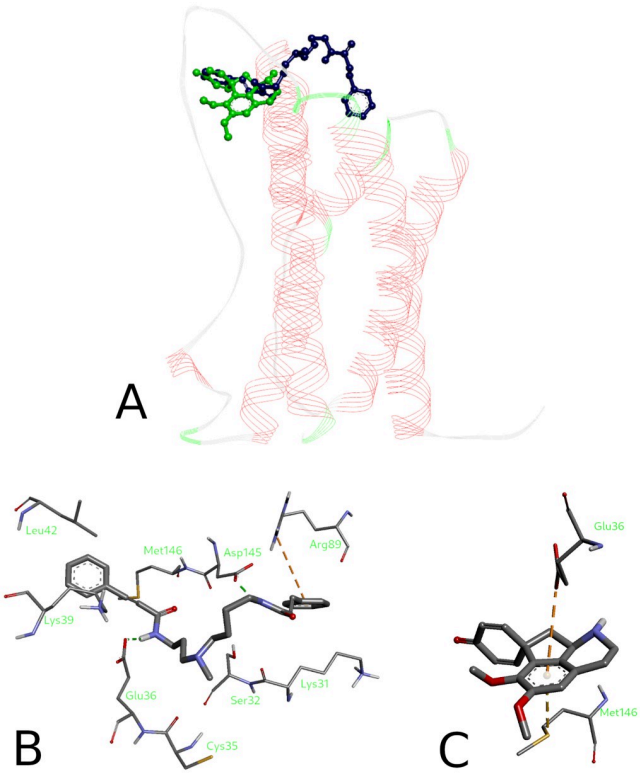

Fig 10. Binding poses (A) of the alkaloids at the IL-6 and their binding modes (B, C). 5-*N*-methylmaytenine (blue A, B) and stepharine (green A, C).

https://doi.org/10.1371/journal.pone.0239364.g010

Conclusion

This is the first paper dealing with 5-*N*-methylmaytenine isolation from natural products and the first report on the occurrence of both 5-*N*-methylmaytenine and stepharine alkaloids in branches of the Amazonian plant *Abuta panurensis*. Inhibitory activity of both alkaloids towards the AChE enzyme was evaluated by spectrophotometry and molecular docking study.

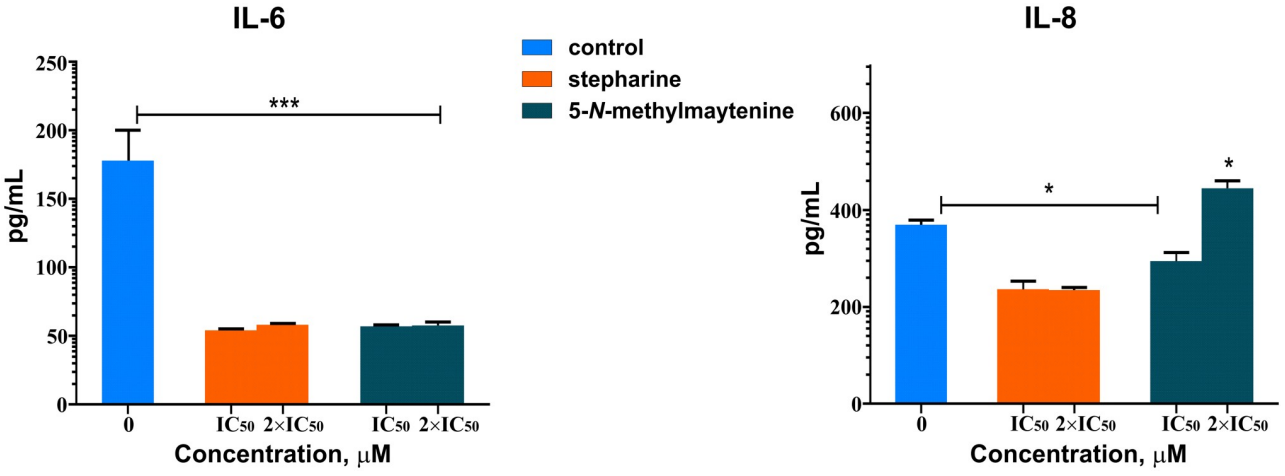

Fig 11. Immunomodulatory effect of 5-*N*-methylmaytenine and stepharine.

https://doi.org/10.1371/journal.pone.0239364.g011

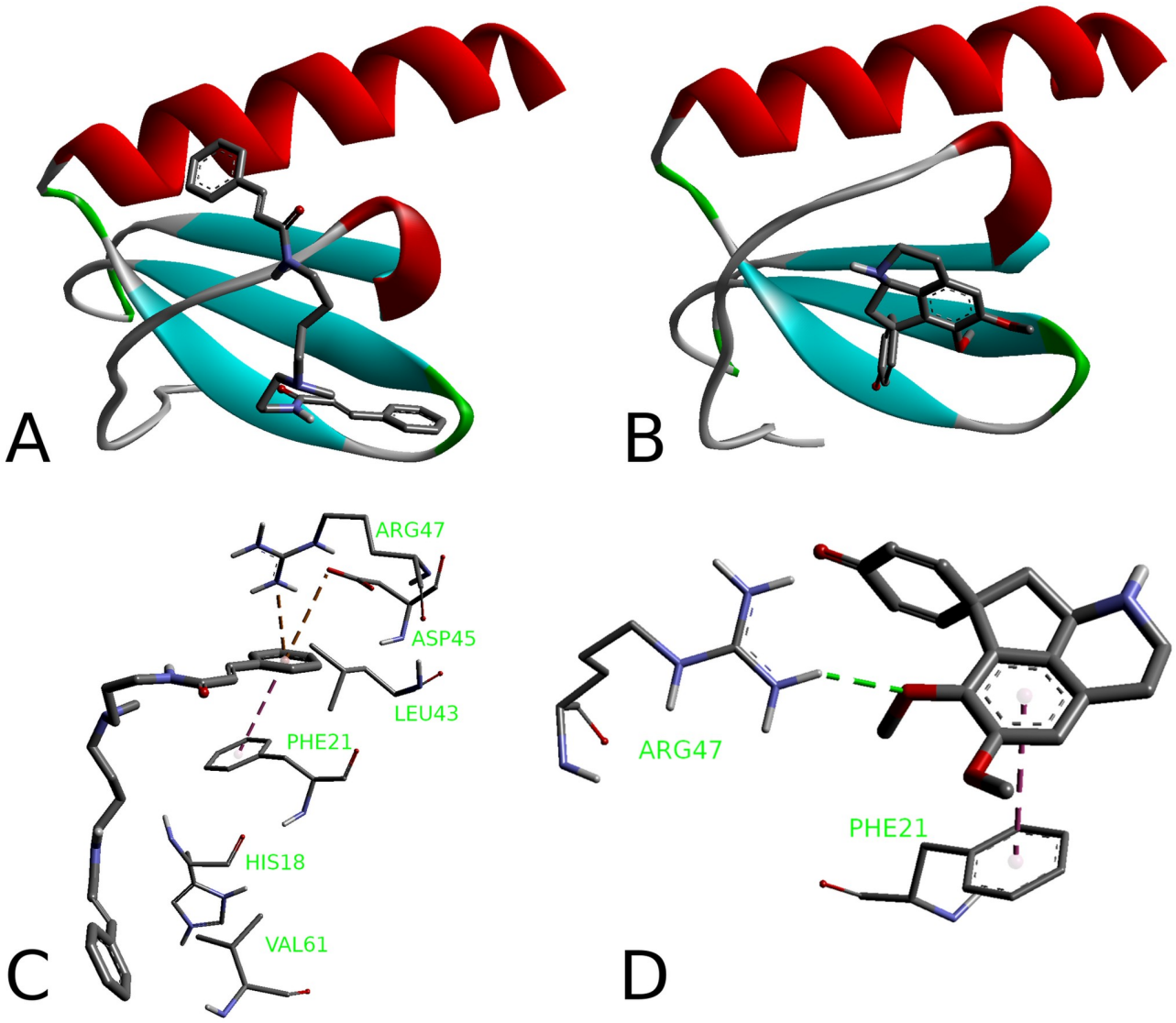

Fig 12. Binding poses (A, B) of the alkaloids at the IL-8 and their binding modes (C, D). 5-*N*-methylmaytenine (A, C) and stepharine (B, D).

https://doi.org/10.1371/journal.pone.0239364.g012

The compounds in question bind effectively to the enzyme active site and demonstrate promising inhibitory potential. Owing to the greater conformational flexibility of 5-*N*-methylmaytenine, it is capable to interact with both anionic and peripheral subsites, thus demonstrating higher AChE inhibition potential, when compared to stepharine.

Both alkaloids were effective against K562 and U937 tumor cells, showing practically no toxicity to normal cell lines Vero and human PBMC.

5-*N*-methylmaytenine and stepharine demonstrated immunomodulatory activity towards IL-6 and IL-8 interleukins. In the former case, both alkaloids inhibited the IL-6 production at very similar levels, which may probably be related to the formation of hydrogen bonds with the protein binding sites. In the latter case, stepharine inhibited considerably the production of IL-8 in comparison to 5-*N*-methylmaytenine that showed a dose dependent action (inhibitory at the IC_{50} dose, and stimulatory at the twofold IC_{50} one). Such a behavior may possibly

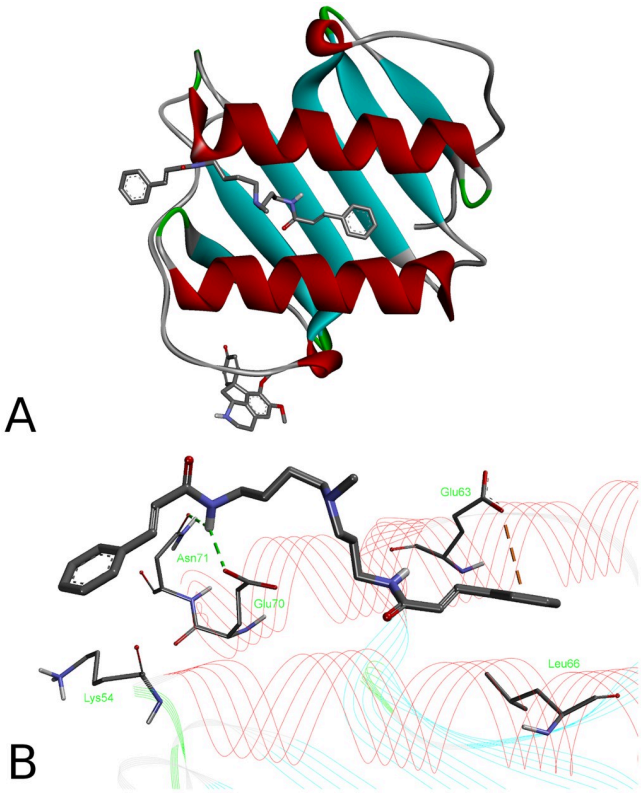

Fig 13. Binding poses of the alkaloids at the IL-8 dimer (A) and binding mode of 5-*N*-methylmaytenine (B). Stepharine-dimer binding mode is similar to the one shown in the Fig 12D.

https://doi.org/10.1371/journal.pone.0239364.g013

be explained by different binding modes of the alkaloids to the interleukin monomer and dimer forms.

Our results suggest that 5-*N*-methylmaytenine and stepharine could be used as reversible AChE inhibitors in the treatment of neurological disorder manifestations, as well as candidate immunomodulatory agents in the inflammatory disease context. However, more research is necessary to better investigate the complete pharmacological potential and toxicological profile of these compounds.

Supporting information

S1 File.
(PDF)

Acknowledgments

The authors express their gratitude to the Analytical Center (UFAM) for assistance in analyses, to Drs M.J. Kato and L. Yamaguchi from the Institute of Chemistry of the University of São Paulo (SP, Brazil) for HRMS analyses, to MSc M.P. Muniz (National Institute for Amazonian Research–INPA, Manaus, AM, Brazil) for his assistance in treatment of HRMS spectra, and to Drs K. Pyrshev (O.V. Palladin Institute of Biochemistry–NAS, Kyiv, Ukraine) and M. Rybak (Institute of Molecular Biology and Genetics–NAS, Kyiv, Ukraine) for valuable discussions.

Author Contributions

Conceptualization: Andriy Grafov.

Data curation: Rochelly da Silva Mesquita, Regiane Costa de Oliveira, Ingrity Suelen Costa Sá, Gabriel Coutinho Borges Camargo, Gemilson Soares Pontes, Felipe Moura Araújo da Silva, Rita de Cássia Saraiva Nunomura.

Formal analysis: Ingrity Suelen Costa Sá, Rita de Cássia Saraiva Nunomura.

Investigation: Rochelly da Silva Mesquita, Andrii Kyrylchuk, Regiane Costa de Oliveira, Ingrity Suelen Costa Sá, Gabriel Coutinho Borges Camargo, Andriy Grafov.

Methodology: Gemilson Soares Pontes, Felipe Moura Araújo da Silva.

Supervision: Rita de Cássia Saraiva Nunomura, Andriy Grafov.

Visualization: Andrii Kyrylchuk.

Writing – original draft: Rochelly da Silva Mesquita, Andrii Kyrylchuk, Gemilson Soares Pontes, Andriy Grafov.

References

1. Barbosa-Filho J, Cunha EVL, Gray A. Alkaloids of the menispermaceae. Press. A, editor. Alkaloids Chem Biol. 2000; 54: 1–190. https://doi.org/10.1016/S0099-9598(00)54002-4
2. Carlquist S. Wood and Stem Anatomy of Menispermaceae. Aliso A J Syst Evol Bot. 1995; 14: 155–170.
3. Manu A, Tanvi S, Anu D, Neeraj B, Ahmad SA. An Inside Review of Cissampelos Pareira LINN: A Potential Medicinal Plant of India. Int Res J Pharm. 2012; 3: 38–41.
4. Sayagh C, Long C, Moretti C, Lavaud C. Saponins and alkaloids from Abuta grandifolia. Phytochem Lett. 2012; 5: 188–193. https://doi.org/10.1016/j.phytol.2011.12.007
5. Menachery MD. The Alkaloids of South American Menispermaceae. Pensylvania, United States; 1998. pp. 269–302.
6. Deevanhxay P, Suzuki M, Maeshibu N, Li H, Tanaka K, Hirose S. Simultaneous characterization of quaternary alkaloids, 8-oxoprotoberberine alkaloids, and a steroid compound in Coscinium fenestratum by liquid chromatography hybrid ion trap time-of-flight mass spectrometry. J Pharm Biomed Anal. 2009; 50: 413–425. https://doi.org/10.1016/j.jpba.2009.05.023 PMID: 19539442
7. Pinheiro MLB, Filho WW, Rocha IDA, Porter B, Wenker E. Abutasterone, an ecdysone from Abuta velutina. Phytochemistry. 1983; 22: 2320–2321.
8. Yu LL, Li RT, Ai YB, Liu W, Deng ZS, Zou ZM. Protoberberine isoquinoline alkaloids from Arcangelisia gusanlung. Molecules. 2014; 19: 13332–13341. https://doi.org/10.3390/molecules190913332 PMID: 25178058
9. Kongkiatpaiboon S, Duangdee N, Prateeptongkum S, Tayana N, Inthakusol W. Simultaneous HPLC analysis of crebanine, dicentrine, stephanine and tetrahydropalmatine in Stephania venosa. Brazilian J Pharmacogn. 2017; 27: 691–697. https://doi.org/10.1016/j.bjp.2017.10.004
10. Damas P, Bruneton J, Fournet A, Guinaudeau H. 2-Norlimacusine, nouvelle bisbenzylisoquinoleine isolee de sciadotenia eichleriana. J Nat Prod. 1985; 48: 69–71. https://doi.org/10.1021/np50037a012
11. Semwal DK, Semwal RB. Efficacy and safety of Stephania glabra: An alkaloid-rich traditional medicinal plant. Nat Prod Res. 2015; 29: 396–410. https://doi.org/10.1080/14786419.2014.955487 PMID: 25186139
12. Bentley KW. B-Phenylethylamines and the Isoquinoline Alkaloids. Nat Prod Rep. 1989; 405–432. https://doi.org/10.1039/np9890600405 PMID: 2674787
13. Hocquemiller R, Cave A. La Saulatine, Alcaloide Isoquinoléique Original Isole de Abuta Bullata. J Nat Prod. 1984.
14. Steele JCP, Simmonds MSJ, Veitch NC, Warhurst DC. Evaluation of the anti-plasmodial activity of bisbenzylisoquinoline alkaloids from Abuta grandifolia. Planta Med. 1999; 65: 413–416. https://doi.org/10.1055/s-1999-14017 PMID: 10418326
15. Duté P, Weber JF, Fournet A, Cavé A, Bruneton J. Bis-benzylisoquinoline alkaloids from Abuta pahni. Phytochemistry. 1987; 26: 2136–2137. https://doi.org/10.1016/S0031-9422(00)81784-7

16. Cava MP, Saa JM, Lakshmikantham MV, Mitchell MJ. Panurensine and Norpanurensine, new bisbenzylisoquinoline alkaloids from Abuta panurensis. J Org Chem. 1975; 40: 2647–2649. https://doi.org/10.1021/jo00906a016 PMID: 1159565

17. Cometa MF, Fortuna S, Palazzino G, Volpe MT, Rengifo Salgado E, Nicoletti M, et al. New cholinesterase inhibiting bisbenzylisoquinoline alkaloids from Abuta grandifolia. Fitoterapia. 2012; 83: 476–480. https://doi.org/10.1016/j.fitote.2011.12.015 PMID: 22230193

18. Ginaudeau H, Leboeuf M, Cavé A. Aporphine alkaloids. II. J Nat Prod. 1979; 42: 325–360. https://doi.org/10.1021/np50004a001 PMID: 5879291

19. Swaffar DS, Holley CJ, Fitch RW, Elkin KR, Zhang C, Sturgill JP, et al. Phytochemical investigation and in vitro cytotoxic evaluation of alkaloids from abuta rufescens. Planta Med. 2012; 78: 230–232. https://doi.org/10.1055/s-0031-1280383 PMID: 22109836

20. Cava MP, Buck K T, Noguchi I, Srinivasan M, Rao MG. The alkaloids of Abuta imene and Abuta rufescens. Tetrahedron. 1975; 31: 4–6.

21. Murebwayire S, Ingkaninan K, Changwijit K, Frédérich M, Duez P. *Triclisia sacleuxii* (Pierre) Diels (Menispermaceae), a potential source of acetylcholinesterase inhibitors. J Pharm Pharmacol. 2008; 61: 103–107. https://doi.org/10.1211/jpp/61.01.0014 PMID: 19126303

22. Houghton PJ, Ren Y, Howes MJ. Acetylcholinesterase inhibitors from plants and fungi. Nat Prod Rep. 2006; 23: 181–199. https://doi.org/10.1039/b508966m PMID: 16572227

23. Rojas Y, Soto R, Amaya E, Retuerto F, Fuertes CM. Efecto antitumoral de los alcaloides hidrosolubles de Abuta grandifolía (MART) Satidwith, en Línea Celular HEP-2. Cienc Invest. 2004; 7: 22–26.

24. Stevigny C, Bailly C, Quetin-Leclercq J. Cytotoxic and Antitumor Potentialities of Aporphinoid Alkaloids. Curr Med Chem Agents. 2005; 5: 173–182. https://doi.org/10.2174/1568011053174864 PMID: 15777224

25. Vieira GC, Gadelha FAAF, Pereira RF, Ferreira LKDP, Barbosa-Filho JM, Bozza PT, et al. Warifteine, an alkaloid of Cissampelos sympodialis, modulates allergic profile in a chronic allergic rhinitis model. Brazilian J Pharmacogn. 2018; 28: 50–56. https://doi.org/10.1016/j.bjp.2017.10.009

26. Cava MP, Nomura K, Talapatra SK, Mitchell MJ, Schlessinger RH, Buck KT, et al. Alkaloids of Stephania glabra. Direct chemical correlation of the absolute configuration of some benzyltetrahydroisoquinoline, proaporphine, and aporphine alkaloids. A protoberberine alkaloid. J Org Chem. 1968; 33: 2785–2789. https://doi.org/10.1021/jo01271a037

27. Dong JW, Cai L, Fang YS, Xiao H, Li ZJ, Ding ZT. Proaporphine and aporphine alkaloids with acetylcholinesterase inhibitory activity from Stephania epigaea. Fitoterapia. 2015; 104: 102–107. https://doi.org/10.1016/j.fitote.2015.05.019 PMID: 26028544

28. Nabavi SMEU, Rastrelli L, Sobarzo-Sánchez E. Aporphines and Alzheimer's Disease: Towards a Medical Approach Facing the Future. Curr Med Chem. 2019; 26: 3253–3259. https://doi.org/10.2174/0929867325666180514102933 PMID: 29756568

29. Kuznetsov YB, Arzamascev EV, Mironova MI, Eliseev AT, Bogonatova LN. Remedies for treatment of traumatic and postoperative damage of peripheral nervous system. 1713151. Russian Federation; 1713151, 1986. http://patents.su/0-1713151-sredstvo-dlya-lecheniya-travmaticheskikh-i-posleoperacionnykh-%0Apovrezhdenijj-perifericheskojj-nervnojj-sistemy.html

30. Lago JHG, Chaves MH, Ayres MCC, Agripino DG, Young MCM. Evaluation of Antifungal and DNA-Damaging Activities of Alkaloids from Branches of Porcelia macrocarpa. Planta Med. 2007; 73: 292–295. https://doi.org/10.1055/s-2007-967108 PMID: 17354171

31. Marks KD. The Total Synthesis of (±) Stepharine. The University of Texas. 2013.

32. Chang F, Hwang T, Yang Y, Li C. Anti-Inflammatory and Cytotoxic Diterpenes from Formosan Polyalthia longifolia var. pendula. Planta Med. 2006; 72: 1344–1347. https://doi.org/10.1055/s-2006-951691 PMID: 17022008

33. Honda T, Shigehisa H. Novel and efficient synthetic path to proaporphine alkaloids: Total synthesis of (±)-stepharine and (±)-pronuciferine. Org Lett. 2006; 8: 657–659. https://doi.org/10.1021/ol052841m PMID: 16468735

34. Bienz S, Bisegger P, Guggisberg A, Hesse M, Hesse M. Polyamine alkaloids. Nat Prod Rep. 2005; 22: 647–658. https://doi.org/10.1039/b413742f PMID: 16193161

35. Ponchet M, Martin-Tanguy J, Marais A, Martin C. Hydroxycinnamoyl acid amides and aromatic amines in the inflorescences of some araceae species. Phytochemistry. 1980; 21: 2865–2869. https://doi.org/10.1016/0031-9422(80)85057-6

36. Bokern M, Witte L, Wray V, Nimtz M, Meurer-Grimes B. Trisubstituted hydroxycinnamic acid spermidines from Quercus dentata pollen. Phytochemistry. 1995; 39: 1371–1375. https://doi.org/10.1016/0031-9422(95)00151-V

37. Kumar V, Bhatt V, Kumar N. Amides From Plants: Structures and Biological Importance. 1st ed. Studies in Natural Products Chemistry. 1st ed. Elsevier B.V.; 2018. pp. 287–333.

38. Niwa T, Doi U, Osawa T. Inhibitory activity of corn-derived bisamide compounds against α-glucosidase. J Agric Food Chem. 2003; 51: 90–94. https://doi.org/10.1021/jf020758x PMID: 12502390

39. Hedberg C, Hesse M, Werner C. Spermine and spermidine hydroxycinnamoyl transferases in Aphelandra tetragona. Plant Sci. 1996; 113: 149–156. https://doi.org/10.1016/0168-9452(95)04298-9

40. Negrel J, Javelle F, Paynot M. Separation of putrescine and spermidine hydroxycinnamoyl transferases extracted from tobacco callus. Phytochemistry. 1991; 30: 1089–1092. https://doi.org/10.1016/S0031-9422(00)95177-X

41. Efdi M, Itoh T, Akao Y, Nozawa Y. The isolation of secondary metabolites and in vitro potent anti-cancer activity of clerodermic acid from Enicosanthum membranifolium. Bioorg Med Chem. 2007; 15: 3667–3671. https://doi.org/10.1016/j.bmc.2007.03.051 PMID: 17400462

42. Martin-Tanguy J, Deshayes A, Perdrizet E, Martin C. Hydroxycinnamic Acid Amides (HCA) in Zea Mays. Distribution and changes with cytoplasmic male sterility. FEBS Lett. 1979; 108: 1–3. https://doi.org/10.1016/0014-5793(79)81164-3 PMID: 230074

43. Schäfer A, Benz H, Fiedler W, Guggisberg A, Bienz S, Hesse M. Polyamine Toxins from Spiders and Wasps. Alkaloids Chem Pharmacol. 1994; 45: 1–125. https://doi.org/10.1016/S0099-9598(08)60276-X PMID: 7535265

44. Clericuzio M, Piovano M, Chamy MC, Garbarino JA, Milanesio M, Viterbo D, et al. Structural Characterisation of Metabolites from Pholiota spumosa (Basidiomycetes). Croat Chem Acta. 2004; 77: 605–611.

45. Tabasso S. Fungal metabolites: Isolation, structural characterization, bioactivity and synthesis. Universita´Degli Studi di Torino. 2007.

46. Clericuzio M, Tabasso S, Garbarino JA, Piovano M, Cardile V, Russo A, et al. Non-phenolic dicinnamamides from Pholiota spumosa: Isolation, synthesis and antitumour activity. European J Org Chem. 2007; 5551–5559. https://doi.org/10.1002/ejoc.200700558

47. Steglich W, Steffan B, Stroech K, Wolf M. Pistillarin, ein charakteristischer Inhaltsstoff und einiger Ramaria -Arten (Basidiomycetes). Z Naturforsch. 1984; 39c: 10–12.

48. Russo A, Piovano M, Clericuzio M, Lombardo L, Tabasso S, Chamy MC, et al. Putrescine-1,4-dicinnamide from Pholiota spumosa (Basidiomycetes) inhibits cell growth of human prostate cancer cells. Phytomedicine. 2007; 14: 185–191. https://doi.org/10.1016/j.phymed.2006.09.010 PMID: 17085028

49. Rosario SL, da Silva A jorge R, Parente JP. Alkamides from Cissampelos glaberrima. Planta Med. 1996; 62: 376–377. https://doi.org/10.1055/s-2006-957913 PMID: 17252475

50. Galarce-Bustos O, Pavón-Pérez J, Henríquez-Aedo K, Aranda M. An improved method for a fast screening of α-glucosidase inhibitors in cherimoya fruit (Annona cherimola Mill.) applying effect-directed analysis via high-performance thin-layer chromatography-bioassay-mass spectrometry. J Chromatogr A. 2019; 1–17. https://doi.org/10.1016/j.chroma.2019.460415 PMID: 31402104

51. Wang J, Cai P, Yang X, Li F, Wu J, Kong L, et al. Novel cinnamamide-dibenzylamine hybrids: Potent neurogenic agents with antioxidant, cholinergic, and neuroprotective properties as innovative drugs for Alzheimer ' s disease. Eur J Med Chem. 2017; 139: 68–83. https://doi.org/10.1016/j.ejmech.2017.07.077 PMID: 28800459

52. Karigiannis G, Papaioannou D. Structure, Biological Activity and Synthesis of Polyamine Analogues and Conjugates. Eur J OrgChem. 200AD; 1841–1863.

53. Saifah E, Suttisri R, Shamsub S, Pengsuparp T. Bisamides from Aglaia edulis. Phytochemistry. 1999; 52: 1085–1088. https://doi.org/10.1016/s0031-9422(99)00378-7 PMID: 10643670

54. von Englert G, Klinga K, Raymond-Hamets, Schlittler E, Vetterl W. Die Struktur von Maytenin. Helv Chim Acta. 1973; 56: 474–478.

55. McManis JS, Ganem B. The Chemistry of Naturally Occurring Polyamines. 1. Total Synthesis of Celacinnine, Celabenzine and Maytenine. J Org Chem. 1980; 45: 2041–2042. https://doi.org/10.1021/jo01298a073

56. Peperidou A, Pontiki E, Hadjipavlou-Litina D, Voulgari E, Avgoustakis K. Multifunctional cinnamic acid derivatives. Molecules. 2017; 22: 1–17. https://doi.org/10.3390/molecules22081247 PMID: 28757554

57. Pedersen HA, Steffensen SK, Christophersen C, Mortensen AG, Jorgensen LN, Niveyro S, et al. Synthesis and Quantitation of Six Phenolic Amides in Amaranthus spp. J Agric Food Chem. 2010; 58: 6306–6311. https://doi.org/10.1021/jf100002v PMID: 20438062

58. Zamble A, Sahpaz S, Hennebelle T, Carato P, F F, Cedex L. N 1, N 5, N 10 -Tris (4-hydroxycinnamoyl) spermidines from Microdesmis keayana Roots. Chem Biodivers. 2006; 3: 982–989. https://doi.org/10.1002/cbdv.200690107 PMID: 17193330

59. Schlittler VE, Spitaler U, Weber Nikolaus. Uber die Synthesen von Maytenin, N-Methylspermidin und N-Methylmaytenin. Helv Chim Acta. 1973; 56: 1097–1099. https://doi.org/10.1002/hlca.19730560330 PMID: 4733350

60. Soares ER, Da Silva FMA, De Almeida RA, De Lima BR, Da Silva Filho FA, Barison A, et al. Direct infusion ESI-IT-MS^n alkaloid profile and isolation of tetrahydroharman and other alkaloids from Bocageopsis pleiosperma maas (Annonaceae). Phytochem Anal. 2015; 26: 339–345. https://doi.org/10.1002/pca.2568 PMID: 26108161

61. Stewart JJP. Optimization of parameters for semiempirical methods VI: More modifications to the NDDO approximations and re-optimization of parameters. J Mol Model. 2013; 19: 1–32. https://doi.org/10.1007/s00894-012-1667-x PMID: 23187683

62. Stewart JJP. MOPAC2016. Stewart Computational Chemistry, Colorado Springs, CO, USA; 2016.

63. Morris GM, Huey R, Lindstrom W, Sanner MF, Belew RK, Goodsell DS, et al. AutoDock4 and AutoDockTools4: Automated docking with selective receptor flexibility. J Comput Chem. 2009; 30: 2785–2791. https://doi.org/10.1002/jcc.21256 PMID: 19399780

64. Sanner MF. Pyton: A Programming Language for Software Integration and Development. J Mol Graph Model. 1999; 17: 57–61. PMID: 10660911

65. Šali A, Blundell TL. Comparative Protein Modelling by Satisfaction of Spatial Restraints. J Mol Biol. 1993; 234: 779–815. https://doi.org/10.1006/jmbi.1993.1626 PMID: 8254673

66. Pettersen EF, Goddard TD, Huang CC, Couch GS, Greenblatt DM, Meng EC, et al. UCSF Chimera?A visualization system for exploratory research and analysis. J Comput Chem. 2004; 25: 1605–1612. https://doi.org/10.1002/jcc.20084 PMID: 15264254

67. Dassault Systèmes BIOVIA, Discovery Studio Visualizer, v19. San Diego: Dassault Systèmes; 2018.

68. Trott O, Olson AJ. AutoDock Vina: Improving the speed and accuracy of docking with a new scoring function, efficient optimization, and multithreading. J Comput Chem. 2010; 31: 455–461. https://doi.org/10.1002/jcc.21334 PMID: 19499576

69. Kumar A, Zhang KYJ. Investigation on the Effect of Key Water Molecules on Docking Performance in CSARdock Exercise. J Chem Inf Model. 2013; 53: 1880–1892. https://doi.org/10.1021/ci400052w PMID: 23617355

70. Schrödinger L. PyMOL. August; 2010.

71. Ellman GL, Courtney KD, Andres V, Featherstone RM. A new and rapid colorimetric determination of acetylcholinesterase activity. Biochem Pharmacol. 1961; 7: 88–95. https://doi.org/10.1016/0006-2952(61)90145-9 PMID: 13726518

72. Senol FS, Orhan IE, Ustun O. In vitro cholinesterase inhibitory and antioxidant effect of selected coniferous tree species. Asian Pac J Trop Med. 2015; 8: 269–275. https://doi.org/10.1016/S1995-7645(14)60329-1 PMID: 25975497

73. Oukoloff K, Coquelle N, Bartolini M, Naldi M, Le Guevel R, Bach S, et al. Design, biological evaluation and X-ray crystallography of nanomolar multifunctional ligands targeting simultaneously acetylcholinesterase and glycogen synthase kinase-3. Eur J Med Chem. 2019; 168: 58–77. https://doi.org/10.1016/j.ejmech.2018.12.063 PMID: 30798053

74. Somers W, Stahl M, Seehra JS. 1.9 Å crystal structure of interleukin 6: Implications for a novel mode of receptor dimerization and signaling. EMBO J. 1997; 16: 989–997. https://doi.org/10.1093/emboj/16.5.989 PMID: 9118960

75. Choy E, Rose-John S. Interleukin-6 as a Multifunctional Regulator: Inflammation, Immune Response, and Fibrosis. J Scleroderma Relat Disord. 2017; 2: S1–S5. https://doi.org/10.5301/jsrd.5000265

76. Boulanger MJ. Hexameric Structure and Assembly of the Interleukin-6/IL-6 -Receptor/gp130 Complex. Science (80-). 2003; 300: 2101–2104. https://doi.org/10.1126/science.1083901 PMID: 12829785

77. Baldwin ET, Weber IT, St. Charles R, Xuan JC, Appella E, Yamada M, et al. Crystal structure of interleukin 8: Symbiosis of NMR and crystallography. Proc Natl Acad Sci U S A. 1991; 88: 502–506. https://doi.org/10.1073/pnas.88.2.502 PMID: 1988949

78. Rajarathnam K, Schnoor M, Richardson RM, Rajagopal S. How do chemokines navigate neutrophils to the target site: Dissecting the structural mechanisms and signaling pathways. Cell Signal. 2019; 54: 69–80. https://doi.org/10.1016/j.cellsig.2018.11.004 PMID: 30465827

79. Gerber N, Lowman H, Artis DR, Eigenbrot C. Receptor-binding conformation of the?ELR? motif of IL-8: X-ray structure of the L5C/H33C variant at 2.35? resolution. Proteins Struct Funct Genet. 2000; 38: 361–367. PMID: 10707023

80. Eigenbrot C, Lowman HB, Chee L, Artis DR. Structural change and receptor binding in a chemokine mutant with a rearranged disulfide: X-ray structure of e38C/C50A IL-8 at 2 Å resolution. Proteins Struct Funct Genet. 1997; 27: 556–566. PMID: 9141135

81. Stévigny C, Jiwan JLH, Rozenberg R, De Hoffmann E, Quetin-Leclercq J. Key fragmentation patterns of aporphine alkaloids by electrospray ionization with multistage mass spectrometry. Rapid Commun Mass Spectrom. 2004; 18: 523–528. https://doi.org/10.1002/rcm.1343 PMID: 14978796

82. Costa EV, Sampaio MFC, Salvador MJ, Nepel A, Barison A. Chemical constituents from the stem bark of Annona pickelii (Annonaceae). Quim Nova. 2015; 38: 769–776. https://doi.org/10.5935/0100-4042.20150069

83. Thuy TT, Porzel A, Franke K, Wessjohann L, Van Sung T. Isoquinolone and protoberberine alkaloids from Stephania rotunda. Pharmazie. 2005; 60: 701–704. https://doi.org/10.1002/chin.200601202 PMID: 16222872

84. Dary C, Bun SS, Herbette G, Mabrouki F, Bun H, Kim S, et al. Chemical profiling of the tuber of Stephania cambodica Gagnep. (Menispermaceae) and analytical control by UHPLC-DAD. Nat Prod Res. 2017; 31: 802–809. https://doi.org/10.1080/14786419.2016.1247077 PMID: 27976592

85. Thornber CW. Alkaloids of the menispermaceae. Phytochemistry. 1970; 9: 157–187. https://doi.org/10.1016/S0031-9422(00)86628-5

86. Blanchfield JT, Sands DPA, Kennard CHL, Byriel KA, Kitching W. Characterisation of alkaloids from some Australian Stephania (Menispermaceae) species. Phytochemistry. 2003; 63: 711–720. https://doi.org/10.1016/s0031-9422(03)00240-1 PMID: 12842145

87. Bartley JP, Baker LT, Carvalho CF. Alkaloids of Stephania bancroftii. Phytochemistry. 1994; 36: 1327–1331. https://doi.org/10.1016/S0031-9422(00)89661-2

88. Shangguan Y, He J, Kang Y, Wang Y, Yang P, Guo J, et al. Structural Characterisation of Alkaloids in Leaves and Roots of Stephania kwangsiensis by LC-QTOF-MS. Phytochem Anal. 2018; 29: 101–111. https://doi.org/10.1002/pca.2718 PMID: 28895207

89. Gorpenchenko TY, Grigorchuk VP, Fedoreyev SA, Tarbeeva DV., Tchernoded GK, Bulgakov VP. Stepharine production in morphogenic cell cultures of Stephania glabra (ROXB.) Miers. Plant Cell Tissue Organ Cult. 2017; 128: 67–76. https://doi.org/10.1007/s11240-016-1083-5

90. Rapp C, Goldberger E, Tishbi N, Kirshenbaum R. Cation-π interactions of methylated ammonium ions: A quantum mechanical study. Proteins Struct Funct Bioinforma. 2014; 82: 1494–1502. https://doi.org/10.1002/prot.24519 PMID: 24464782

91. Dvir H, Silman I, Harel M, Rosenberry TL, Sussman JL. Acetylcholinesterase: From 3D structure to function. Chem Biol Interact. 2010; 187: 10–22. https://doi.org/10.1016/j.cbi.2010.01.042 PMID: 20138030

92. de Lima BR, Lima JM, Maciel JB, Valentim CQ, Nunomura R de CS, Lima ES, et al. Synthesis and Inhibition Evaluation of New Benzyltetrahydroprotoberberine Alkaloids Designed as Acetylcholinesterase Inhibitors. Front Chem. 2019; 7. https://doi.org/10.3389/fchem.2019.00629 PMID: 31620424

93. Sussman J, Harel M, Frolow F, Oefner C, Goldman A, Toker L, et al. Atomic structure of acetylcholinesterase from Torpedo californica: a prototypic acetylcholine-binding protein. Science (80-). 1991; 253: 872–879. https://doi.org/10.1126/science.1678899 PMID: 1678899

94. Melchiorre C, Andrisano V, Bolognesi ML, Budriesi R, Cavalli A, Cavrini V, et al. Acetylcholinesterase noncovalent inhibitors based on a polyamine backbone for potential use against Alzheimer's disease [2]. J Med Chem. 1998; 41: 4186–4189. https://doi.org/10.1021/jm9810452 PMID: 9784091

95. Inestrosa NC, Alvarez A, Pérez CA, Moreno RD, Vicente M, Linker C, et al. Acetylcholinesterase Accelerates Assembly of Amyloid-β-Peptides into Alzheimer's Fibrils: Possible Role of the Peripheral Site of the Enzyme. Neuron. 1996; 16: 881–891. https://doi.org/10.1016/s0896-6273(00)80108-7 PMID: 8608006

96. Zhang J, Chen L, Sun J. Oxoisoaporphine Alkaloids: Prospective Anti-Alzheimer's Disease, Anticancer, and Antidepressant Agents. ChemMedChem. 2018; 13: 1262–1274. https://doi.org/10.1002/cmdc.201800196 PMID: 29696800

97. Williams P, Sorribas A, Howes M-JR. Natural products as a source of Alzheimer's drug leads. Nat Prod Rep. 2011; 28: 48–77. https://doi.org/10.1039/c0np00027b PMID: 21072430

98. Zhao H, Zhou S, Zhang M, Feng J, Wang S, Wang D, et al. An in vitro AChE inhibition assay combined with UF-HPLC-ESI-Q-TOF/MS approach for screening and characterizing of AChE inhibitors from roots of Coptis chinensis Franch. J Pharm Biomed Anal. 2016; 120: 235–240. https://doi.org/10.1016/j.jpba.2015.12.025 PMID: 26760241

99. Miller-Fleming L, Olin-Sandoval V, Campbell K, Ralser M. Remaining Mysteries of Molecular Biology: The Role of Polyamines in the Cell. J Mol Biol. 2015; 427: 3389–3406. https://doi.org/10.1016/j.jmb.2015.06.020 PMID: 26156863

100. Gilad GM, Gilad VH. Early polyamine treatment enhances survival of sympathetic neurons after postnatal axonal injury or immunosympathectomy. Dev Brain Res. 1988; 38: 175–181. https://doi.org/10.1016/0165-3806(88)90042-9

101. Morrison LD, Kish SJ. Brain polyamine levels are altered in Alzheimer's disease. Neurosci Lett. 1995. https://doi.org/10.1016/0304-3940(95)11881-V

102. Yadav M, Parle M, Jindal DK, Sharma N. Potential effect of spermidine on GABA, dopamine, acetylcholinesterase, oxidative stress and proinflammatory cytokines to diminish ketamine-induced psychotic symptoms in rats. Biomed Pharmacother. 2018; 98: 207–213. https://doi.org/10.1016/j.biopha.2017.12.016 PMID: 29268241

103. Colovic MB, Krstic DZ, Lazarevic-Pasti TD, Bondzic AM, Vasic VM. Acetylcholinesterase Inhibitors: Pharmacology and Toxicology. Curr Neuropharmacol. 2013; 11: 315–335. https://doi.org/10.2174/1570159X11311030006 PMID: 24179466

104. Lin CC, Ng LT, Hsu FF, Shieh DE, Chiang LC. Cytotoxic effects of Coptis chinensis and Epimedium sagittatum extracts and their major constituents (berberine, coptisine and icariin) on hepatoma and leukaemia cell growth. Clin Exp Pharmacol Physiol. 2004; 31: 65–69. https://doi.org/10.1111/j.1440-1681.2004.03951.x PMID: 14756686

105. Letašiová S, Jantová S, Čipák L, Múčková M. Berberine-antiproliferative activity in vitro and induction of apoptosis/necrosis of the U937 and B16 cells. Cancer Lett. 2006; 239: 254–262. https://doi.org/10.1016/j.canlet.2005.08.024 PMID: 16229943

106. Uadkla O, Yodkeeree S, Buayairaksa M, Meepowpan P, Nuntasaen N, Limtrakul P, et al. Antiproliferative effect of alkaloids *via* cell cycle arrest from *Pseuduvaria rugosa*. Pharm Biol. 2013; 51: 400–404. https://doi.org/10.3109/13880209.2012.734314 PMID: 23406361

107. Qing Z-X, Huang J-L, Yang X-Y, Liu J-H, Cao H-L, Xiang F, et al. Anticancer and Reversing Multidrug Resistance Activities of Natural Isoquinoline Alkaloids and their Structure-activity Relationship. Curr Med Chem. 2018; 25: 5088–5114. https://doi.org/10.2174/0929867324666170920125135 PMID: 28933285

108. Borovikova L V., Ivanova S, Zhang M, Yang H, Botchkina GI, Watkins LR, et al. Vagus nerve stimulation attenuates the systemic inflammatory response to endotoxin. Nature. 2000. https://doi.org/10.1038/35013070 PMID: 10839541

109. Wang X, Fang H, Huang Z, Shang W, Hou T, Cheng A, et al. Imaging ROS signaling in cells and animals. Journal of Molecular Medicine. 2013. pp. 917–927. https://doi.org/10.1007/s00109-013-1067-4 PMID: 23873151

110. Sun P, Zhou K, Wang S, Li P, Chen S, Lin G, et al. Involvement of MAPK/NF-κB Signaling in the Activation of the Cholinergic Anti-Inflammatory Pathway in Experimental Colitis by Chronic Vagus Nerve Stimulation. PLoS One. 2013; 8: 1–15. https://doi.org/10.1371/journal.pone.0069424 PMID: 23936328

111. Kaltschmidt B, Uherek M, Wellmann H, Volk B, Kaltschmidt C. Inhibition of NF-κB potentiates amyloid β-mediated neuronal apoptosis. Proc Natl Acad Sci U S A. 1999; 96: 9409–14. https://doi.org/10.1073/pnas.96.16.9409 PMID: 10430956

112. Ross R. The pathogenesis of atherosclerosis: A perspective for the 1990s. Nature. 1993. https://doi.org/10.1038/362801a0 PMID: 8479518

113. Tak PP, Firestein GS. NF-κB: A key role in inflammatory diseases. Journal of Clinical Investigation. 2001. pp. 7–11. https://doi.org/10.1172/JCI11830 PMID: 11134171

114. Rajarathnam K, Prado GN, Fernando H, Clark-Lewis I, Navarro J. Probing Receptor Binding Activity of Interleukin-8 Dimer Using a Disulfide Trap †. Biochemistry. 2006; 45: 7882–7888. https://doi.org/10.1021/bi0605944 PMID: 16784240

115. Lowman HB, Fairbrother WJ, Slagle PH, Kabakoff R, Hebert CA, Liu J, et al. Monomeric variants of IL-8: Effects of side chain substitutions and solution conditions upon dimer formation. Protein Sci. 2008; 6: 598–608. https://doi.org/10.1002/pro.5560060309 PMID: 9070442

116. Nasser MW, Raghuwanshi SK, Grant DJ, Jala VR, Rajarathnam K, Richardson RM. Differential Activation and Regulation of CXCR1 and CXCR2 by CXCL8 Monomer and Dimer. J Immunol. 2009; 183: 3425–3432. https://doi.org/10.4049/jimmunol.0900305 PMID: 19667085

117. Papanicolaou DA, Wilder RL, Manolagas SC, Chrousos GP. The pathophysiologic roles of interleukin-6 in human disease. Annals of Internal Medicine. 1998. pp. 127–37. https://doi.org/10.7326/0003-4819-128-2-199801150-00009 PMID: 9441573

118. Mehta VK, Verma R, Garg RK, Malhotra HS, Sharma PK, Jain A. Study of interleukin-6 and interleukin-8 levels in patients with neurological manifestations of dengue. J Postgrad Med. 2017; 63: 11–15. https://doi.org/10.4103/0022-3859.188545 PMID: 28079042

119. Bonfield TL, Panuska JR, Konstan MW, Hilliard KA, Hilliard JB, Ghnaim H, et al. Inflammatory cytokines in cystic fibrosis lungs. Am J Respir Crit Care Med. 1995; 152: 2111–8. https://doi.org/10.1164/ajrccm.152.6.8520783 PMID: 8520783